microarray analysis with axotomized purified RGCs shows that significant changes in gene expression are an essential aspect of the growth phase of axotomized RGCs (Fischer et al., 2004). These data suggest that 3 days after axotomy is a critical time point for determining the fate of RGCs.

The effect of GDNF on axonal growth was previously reported to be weak in vitro (Yin et al., 2003), and, in agreement with this finding, we found that GDNF and NRTN have no effects on axonal growth. Unlike GDNF and NRTN, ARTN promotes axonal growth in mature RGCs and might play a similar role in development, as suggested by the high levels of GFRα3 expression during development and in the early postnatal period when RGCs are forming their connections and decline in maturity. ARTN has also been shown to activate axonal growth in the mature DRG via SFK- and extracellular signal-related kinase-dependent signaling pathways (Jeong et al., 2008). Like ARTN, Bcl-2-associated athanogene-1 has been reported to have dual effects on neuroprotection and axonal growth in axotomized RGCs, inducing a translocation of Raf-1 and ROCK2 and interaction with the inhibitory ROCK signaling cascade, which results in dual effects on the prevention of apoptosis and axonal regrowth (Planchamp et al., 2008). Phosphotase and tensin homolog gene deletion also stimulates both RGC survival and axon regeneration after axotomy. (Park et al., 2008) Thus, although several factors have been reported to stimulate axon outgrowth alone (oncomodulin; Kurimoto et al., 2010) or survival alone (e.g., bcl2 overexpression [Chierzi et al., 1999], GDNF [this study], and BDNF [Pernet and Di Polo, 2006]), ARTN is among the factors that stimulate both cell survival and axonal growth. In conclusion, we have demonstrated that increased expression of GFRα3 and ARTN stimulate axonal growth both in vivo and in vitro. Additional study using anti-ARTN antibodies, a specific inhibitor of GFRα3, or GFRα3-deficient mice will be required to conclude that this pathway was critical for axon regeneration after nerve crush. However, the GFRα3-dependent pathway may be an attractive target to stimulate the survival and regenerative capacity of RGCs following optic nerve injury.

ACKNOWLEDGMENTS

The authors thank Prof. Larry Benowitz for important comment and discussion, Mrs. Junko Sato for technical assistance, and Mr. Tim Hilts for editing the manuscript.

REFERENCES

Baloh RH, Enomoto H, Johnson EM Jr, Milbrandt J. 2000. The GDNF family ligands and receptors: implications for neural development. Curr Opin Neurobiol 10:103–110.

Brantley MA Jr, Jain S, Barr EE, Johnson EM Jr, Milbrandt J. 2008. Neurturin-mediated ret activation is required for retinal function. J Neurosci 28:4123–4135.

Carmillo P, Dago L, Day ES, Worley DS, Rossomando A, Walus L, Orozco O, Buckley C, Miller S, Tse A, Cate RL, Rosenblad C, Sah DW, Gronborg M, Whitty A. 2005. Glial cell line-derived neurotrophic factor (GDNF) receptor alpha-1 (GFR alpha 1) is highly selective for GDNF versus artemin. Biochemistry 44:2545–2554.

Chierzi S, Strettoi E, Cenni MC, Maffei L. 1999. Optic nerve crush: axonal responses in wild-type and bcl-2 transgenic mice. J Neurosci 19: 8367–8376.

Fischer D, Petkova V, Thanos S, Benowitz LI. 2004. Switching mature retinal ganglion cells to a robust growth state in vivo: gene expression and synergy with RhoA inactivation. J Neurosci 24:8726–8740.

Hauck SM, Kinkl N, Deeg CA, Swiatek-de Lange M, Schoffmann S, Ueffing M. 2006. GDNF family ligands trigger indirect neuroprotective signaling in retinal glial cells. Mol Cell Biol 26:2746–2757.

Jeong DG, Park WK, Park S. 2008. Artemin activates axonal growth via SFK- and ERK-dependent signalling pathways in mature dorsal root ganglia neurons. Cell Biochem Funct 26:210–220.

Koeberle PD, Bahr M. 2008. The upregulation of GLAST-1 is an indirect antiapoptotic mechanism of GDNF and neurturin in the adult CNS. Cell Death Differ 15:471–483.

Koeberle PD, Ball AK. 2002. Neurturin enhances the survival of axotomized retinal ganglion cells in vivo: combined effects with glial cell line-derived neurotrophic factor and brain-derived neurotrophic factor. Neuroscience 110:555–567.

Kurimoto T, Ishii M, Tagami Y, Nishimura M, Miyoshi T, Tsukamoto Y, Mimura O. 2006. Xylazine promotes axonal regeneration in the crushed optic nerve of adult rats. Neuroreport 17:1525–1529.

Kurimoto T, Yin Y, Omura K, Gilbert HY, Kim D, Cen LP, Moko L, Kugler S, Benowitz LI. 2010. Long-distance axon regeneration in the mature optic nerve: contributions of oncomodulin, cAMP, and pten gene deletion. J Neurosci 30:15654–15663.

Lin LF, Doherty DH, Lile JD, Bektesh S, Collins F. 1993. GDNF: a glial cell line-derived neurotrophic factor for midbrain dopaminergic neurons. Science 260:1130–1132.

Lindahl M, Timmusk T, Rossi J, Saarma M, Airaksinen MS. 2000. Expression and alternative splicing of mouse Gfra4 suggest roles in endocrine cell development. Mol Cell Neurosci 15:522–533.

Nakazawa T, Nakano I, Furuyama T, Morii H, Tamai M, Mori N. 2000. The SCG10-related gene family in the developing rat retina: persistent expression of SCLIP and stathmin in mature ganglion cell layer. Brain Res 861:399–407.

Nakazawa T, Nakano I, Sato M, Nakamura T, Tamai M, Mori N. 2002a. Comparative expression profiles of Trk receptors and Shc-related phosphotyrosine adapters during retinal development: potential roles of N-Shc/ShcC in brain-derived neurotrophic factor signal transduction and modulation. J Neurosci Res 68:668–680.

Nakazawa T, Tamai M, Mori N. 2002b. Brain-derived neurotrophic factor prevents axotomized retinal ganglion cell death through MAPK and PI3K signaling pathways. Invest Ophthalmol Vis Sci 43:3319–3326.

Nakazawa T, Shimura M, Tomita H, Akiyama H, Yoshioka Y, Kudou H, Tamai M. 2003. Intrinsic activation of PI3K/Akt signaling pathway and its neuroprotective effect against retinal injury. Curr Eye Res 26:55–63.

Nakazawa T, Morii H, Tamai M, Mori N. 2005a. Selective upregulation of RB3/stathmin4 by ciliary neurotrophic factor following optic nerve axotomy. Brain Res 861:399–407.

Nakazawa T, Shimura M, Endo S, Takahashi H, Mori N, Tamai M. 2005b. N-methyl-D-aspartic acid suppresses Akt activity through protein phosphatase in retinal ganglion cells. Mol Vis 11:1173–1182.

Nakazawa T, Takahashi H, Nishijima K, Shimura M, Fuse N, Tamai M, Hafezi-Moghadam A, Nishida K. 2007. Pitavastatin prevents NMDA-induced retinal ganglion cell death by suppressing leukocyte recruitment. J Neurochem 100:1018–1031.

Ozden S, Isenmann S. 2004. Neuroprotective properties of different anesthetics on axotomized rat retinal ganglion cells in vivo. J Neurotrauma 21:73–82.

Park KK, Liu K, Hu Y, Smith PD, Wang C, Cai B, Xu B, Connolly L, Kramvis I, Sahin M, He Z. 2008. Promoting axon regeneration in the adult CNS by modulation of the PTEN/mTOR pathway. Science 322:963–966.

Pernet V, Di Polo A. 2006. Synergistic action of brain-derived neurotrophic factor and lens injury promotes retinal ganglion cell survival but leads to optic nerve dystrophy in vivo. Brain 129:1014–1026.

Planchamp V, Bermel C, Tonges L, Ostendorf T, Kugler S, Reed JC, Kermer P, Bahr M, Lingor P. 2008. BAG1 promotes axonal outgrowth and regeneration in vivo via Raf-1 and reduction of ROCK activity. Brain 131:2606–2619.

Sariola H, Saarma M. 2003. Novel functions and signalling pathways for GDNF. J Cell Sci 116:3855–3862.

Trupp M, Scott R, Whittemore SR, Ibanez CF. 1999. Ret-dependent and -independent mechanisms of glial cell line-derived neurotrophic factor signaling in neuronal cells. J Biol Chem 274:20885–20894.

Wang JT, Kunzevitzky NJ, Dugas JC, Cameron M, Barres BA, Goldberg JL. 2007. Disease gene candidates revealed by expression profiling of retinal ganglion cell development. J Neurosci 27:8593–8603.

Ward MS, Khoobehi A, Lavik EB, Langer R, Young MJ. 2007. Neuroprotection of retinal ganglion cells in DBA/2J mice with GDNF-loaded biodegradable microspheres. J Pharm Sci 96:558–568.

Worby CA, Vega QC, Chao HH, Seasholtz AF, Thompson RC, Dixon JE. 1998. Identification and characterization of GFRalpha-3, a novel coreceptor belonging to the glial cell line-derived neurotrophic receptor family. J Biol Chem 273:3502–3508.

Yin Y, Cui Q, Li Y, Irwin N, Fischer D, Harvey AR, Benowitz LI. 2003. Macrophage-derived factors stimulate optic nerve regeneration. J Neurosci 23:2284–2293.

Yin Y, Henzl MT, Lorber B, Nakazawa T, Thomas TT, Jiang F, Langer R, Benowitz LI. 2006. Oncomodulin is a macrophage-derived signal for axon regeneration in retinal ganglion cells. Nat Neurosci 9:843–852.

Clinical Ophthalmology

Dovepress
open access to scientific and medical research

Open Access Full Text Article

ORIGINAL RESEARCH

The effect of intravitreal bevacizumab on ocular blood flow in diabetic retinopathy and branch retinal vein occlusion as measured by laser speckle flowgraphy

Fumihiko Nitta[1]
Hiroshi Kunikata[1,2]
Naoko Aizawa[1]
Kazuko Omodaka[1]
Yukihiro Shiga[1]
Masayuki Yasuda[1]
Toru Nakazawa[1–3]

[1]Department of Ophthalmology, Tohoku University Graduate School of Medicine, Sendai, Japan; [2]Department of Retinal Disease Control, Tohoku University Graduate School of Medicine, Sendai, Japan; [3]Department of Advanced Ophthalmic Medicine, Tohoku University Graduate School of Medicine, Sendai, Japan

Background: This study evaluated the effect of intravitreal injection of bevacizumab (IVB) on macular edema associated with diabetic retinopathy (DME) or branch retinal vein occlusion (BRVOME) using laser speckle flowgraphy.

Methods: A comparative interventional study of 25 eyes from 22 patients with macular edema (DME group: 12 eyes; BRVOME group: 13 eyes) who underwent IVB. Mean blur rate (MBR) was measured in the retinal artery, retinal vein, optic nerve head (ONH), and choroid before and after IVB.

Results: In the BRVOME group, there was no significant change in MBR in the retinal artery, retinal vein or ONH, but choroidal MBR decreased significantly (P=0.04). In the DME group, the MBR in the retinal artery, retinal vein, ONH, and choroid decreased significantly (P=0.02, P=0.04, $P<0.001$, and P=0.04, respectively). In the DME group, pre-IVB MBR in the ONH was significantly correlated with post-IVB foveal thickness (R= −0.71, P=0.002). There was no such correlation in the BRVOME group in the ONH.

Conclusion: IVB had a suppressive effect on circulation in eyes with DME but not in those with BRVOME. This suggests that this noninvasive and objective biomarker may be a useful part of pre-IVB evaluations and decision-making in DME.

Keywords: macular edema, mean blur rate, optic nerve head, biomarker, ocular circulation

Introduction

Macular edema is one of the main causes of reduced vision in various retinal diseases, including diabetic retinopathy (DR) and branch retinal vein occlusion (BRVO).[1–4] This condition is difficult to treat successfully, even for experienced ophthalmologists. Currently, intravitreal injection of bevacizumab (IVB), an anti-vascular endothelial growth factor (VEGF) antibody, is one of the most accepted treatments.[5–8] It can improve vision by temporarily blocking VEGF action and subsequently reducing macular edema. However, in cases of DR- or BRVO-associated macular edema (DME and BRVOME, respectively), the effect of IVB is often insufficient, requiring the treatment to be repeated many times.[8–11] It is not known why the effectiveness of the treatment is poor in these cases, as the underlying mechanism of IVB's ability to reduce macular edema is still not well understood. Furthermore, the effect of IVB on retinal circulation is also unknown, although there are a few reports that IVB causes a decrease in intraocular and systemic circulation.[12,13] Particularly, IVB can adversely affect the visual prognosis of patients with central retinal vein occlusion and underlying systemic diseases such as diabetes, or ischemic heart or cerebrovascular diseases.[14,15]

Correspondence: Hiroshi Kunikata
Department of Ophthalmology, Tohoku University Graduate School of Medicine, 1-1 Seiryo-machi, Aoba-ku, Sendai 980-8574, Japan
Tel +81 22 717 7294
Fax +81 22 717 7298
Email kunikata@oph.med.tohoku.ac.jp

submit your manuscript | www.dovepress.com
Dovepress
http://dx.doi.org/10.2147/OPTH.S62022

Ischemic change after any medical intervention is ordinarily evaluated with fluorescein angiography, but this technique is invasive, can cause severe complications, including anaphylactic shock, and its results can be affected by time-dependent changes after injection. Recent innovations in an alternative technique, laser speckle flowgraphy (LSFG), have allowed us to quickly and easily monitor changes in tissue circulation over time.[16,17] The main measurement parameter of LSFG, mean blur rate (MBR), is an automatically calculated index of ocular blood flow derived from the scatter pattern produced when the ocular fundus is irradiated with laser light. MBR represents the velocity of the blurring in the speckle pattern that is caused by blood flow. Measured values of MBR correlate well with absolute blood flow values measured with the hydrogen gas clearance and microsphere methods.[18,19] Previous reports have shown that despite being a relative value, MBR can be considered an accurate representation of both ocular blood flow and velocity.[20,21] The quality of LSFG measurements mainly relies on the clarity of the ocular media, but LSFG has already contributed to many recent findings in glaucoma research, and is especially useful in examining the relationship between glaucoma and ocular circulation.[16,22–25]

In this study, we hypothesized that IVB had a different effect on ocular blood circulation in DME and BRVOME. We evaluated the association between MBR and clinical findings in post-IVB eyes in order to reveal the different pathogenesis of DME and BRVOME, and to find new biomarkers of post-IVB visual prognosis. Thus, our purpose was to evaluate the effect of IVB in DME and BRVOME patients by examining the association of MBR and clinical findings related to the structure and function of the retina.

Materials and methods

Setting and design

This was an institutional, prospective, nonrandomized, interventional case series. Subjects were recruited from patients referred to the Retina Service of Tohoku University Hospital. Intravitreal intervention and follow-up were both performed at this clinic.

Patients

The study comprised 25 eyes of 22 patients (eleven men and eleven women, mean age: 67.5 years) with retinal disease (DR group: 12 eyes of nine patients with DR; BRVO group: 13 eyes of 13 patients with BRVO) and macular edema.

Each patient provided informed consent for their participation in this study as well as for the treatments they received. The study was approved by the institutional review board of Tohoku University Graduate School of Medicine (Protocol No 2013-164; May 17, 2013). The research was conducted according to the provisions of the Declaration of Helsinki, 1995 (as revised in Edinburgh, 2000).[26,27]

Intervention

In all eyes, after instillation of topical anesthetic (0.4% oxybuprocaine hydrochloride; Benoxil), sterilization of the eyelid (10% povidone-iodine Swabstick), and instillation of 1.25% povidone-iodine (Isodine), 1.25 mg/0.05 mL of bevacizumab (Avastin) was injected into the vitreous cavity with a standard pars plana approach (3.5 mm posterior to the limbus) using a 30-gauge needle.

Measurement of clinical findings

We measured best-corrected visual acuity (BCVA) before, 1 week after, and 1 month after IVB. Similarly, we measured foveal thickness (FT) before, 1 week after, and 1 month after IVB. BCVA was measured with a logMAR chart (5 m) (LVC-10; NEITZ Instruments, Tokyo, Japan), and retinal thickness was measured with optical coherence tomography (OCT) (OCT3000; Carl Zeiss Meditec AG, Jena, Germany). The retinal thickness of the central fovea was defined as the distance between the inner limiting membrane and the retinal pigment epithelium, and was automatically calculated by the OCT3000 software. A macular thickness map was made with the OCT retinal mapping program from six radial scans intersecting at the fovea. The mean retinal thickness was calculated in nine regions: the 1,000 μm central area and the four quadrants of the inner and outer rings. FT was defined as the value of the 1,000 μm central area. Blood pressure and intraocular pressure (IOP) were measured after 10 minutes of rest.

Measurement using laser speckle flowgraphy

We measured MBR with the LSFG NAVI system (Softcare Co., Ltd., Fukutsu, Japan) before, 1 week after, and 1 month after IVB. The measurement conditions were kept constant as follows: angle of view, 21°; number of pixels measured, 750×360; and laser power, 1.37 mW. Determination of MBR was made with LSFG Analyzer software (version 3.0.47.0; Softcare Co., Fukutsu, Japan). We measured four regions: a selected retinal artery, a selected retinal vein, the optic nerve head (ONH), and the choroid. Measurements for the retinal artery and the retinal vein were taken from sites near the ONH (within 1.5 papilla

diameters). In patients with BRVOME, blood vessels in the quadrant containing the obstruction were not selected in order to avoid the influence of the hemorrhage. The mean number of samples was 1,013, 1,482.3, and 47,785.2 in the retinal artery, the retinal vein, and the ONH, respectively. Measurement of the choroid was performed in a square area (150×150 pixels; 19,479 samples) not containing retinal blood vessels, in a temporal location located one papilla diameter away from the ONH. Only a single measurement of each region was performed.

Statistical analysis

Analysis was done with Ekuseru-Toukei 2006 software (Social Survey Research Information Co., Ltd., Tokyo, Japan). The data are presented as mean ± standard deviation. The significance of the difference between pre- and post-IVB data was assessed with the Friedman test and Scheffe's paired comparison. We also used the Mann–Whitney *U* test to compare characteristics other than sex and optic media and clinical findings before and after IVB in the BRVO and DR groups. Sex and optic media were compared with Fisher's exact test. The Spearman correlation coefficient was used to determine the relationship between MBR and FT in the ONH. A *P*-value of less than 0.05 was considered to be statistically significant.

Results

A comparison of characteristics and findings before and after IVB in the BRVOME and DME groups is shown in Table 1. Before IVB, there were no significant differences in age, optic media, IOP, or FT between the two groups, but there were significant differences in sex distribution and visual acuity. After IVB, there was no difference in IOP between the two groups, but there was a significant difference in FT. FT in the BRVOME group was significantly lower than in the DME group 1 month post-IVB.

BCVA and FT before and after IVB are shown in Figures 1 and 2, respectively. MBR in the retinal artery, retinal vein, ONH, and choroid before and after IVB is shown in Figure 3. In the DME group, MBR changed significantly in all regions 1 week and 1 month after IVB (retinal artery, $P=0.02$; retinal vein, $P=0.04$; ONH, $P<0.001$; and choroid, $P=0.04$). In the BRVOME group, MBR did not change significantly 1 week or 1 month after IVB in any of the measured regions (retinal artery, $P=0.09$; retinal vein, $P=0.33$; ONH, $P=0.50$), except the choroid ($P=0.04$).

The relationship between FT and MBR in the ONH of the DME group is shown in Figure 4. Pre-IVB MBR in the ONH was not correlated with pre-IVB FT ($P=0.33$), but post-IVB MBR in the ONH was correlated with post-IVB FT ($R=-0.80$, $P=0.009$). Furthermore, pre-IVB MBR in the ONH was correlated with post-IVB FT ($R=-0.71$, $P=0.002$). The relationship between FT and MBR in the ONH of the BRVOME group is shown in Figure 5. There were no equivalent correlations in the ONH of the BRVOME group.

Representative eyes with DME and BRVOME are shown in Figures 6 and 7, respectively.

Complications arising from IVB, such as endophthalmitis, ocular hypertension, retinal detachment, and vitreous hemorrhage, did not occur in any of the patients in this study.

Table 1 Comparison of characteristics and findings before and after intravitreal injection of bevacizumab in groups with branch retinal vein occlusion and diabetic retinopathy

Group	BRVOME	DME	*P*-value
Number of eyes	13	12	
Age	71.0±9.6	63.8±9.2	0.0565[a]
Sex (M: F)	(4:9)	(7:2)	*0.0402[b]
Optic media (lens: pseudophakia)	(11:1)	(10:3)	0.3278[b]
BCVA (logMAR)			
Pre-IVB	0.8±0.26	0.41±0.21	**0.0016[a]
1 week post-IVB	0.64±0.4	0.49±0.23	0.3355[a]
1 month post-IVB	0.64±0.33	0.45±0.29	0.1245[a]
IOP (mmHg)			
Pre-IVB	13.6±2.4	12.8±1.5	0.2409[a]
1 week post-IVB	12.1±2.3	13.4±2.3	0.1818[a]
1 month post-IVB	12.9±2.1	12.6±2.2	0.8062[a]
Foveal thickness (μm)			
Pre-IVB	549.8±127.7	465.7±120.1	0.0727[a]
1 week post-IVB	327.5±110.1	396.8±116.1	0.2108[a]
1 month post-IVB	270.2±67.9	408.3±148.6	**0.0036[a]

Notes: [a]Mann–Whitney *U* test; [b]Fisher's exact test. *$P<0.05$; **$P<0.01$.
Abbreviations: BCVA, best-corrected visual acuity; BRVOME, branch retinal vein occlusion-associated macular edema; DME, diabetic macular edema; IOP, intraocular pressure; IVB, intravitreal bevacizumab; logMAR, logarithm of the minimum angle resolution; M, male; F, female.

Discussion

We set out to investigate the effect of IVB on the retina in DME and BRVOME patients, in particular its effect on ocular blood flow. We found that in BRVOME patients, there was no significant change in MBR in any of the areas measured in this study, with the exception of a significant decrease in the choroid. In the group of patients with DME, there was a significant decrease in MBR in all measured areas. Interestingly, however, we observed that pre-IVB MBR in the DME patients was significantly correlated with post-IVB FT; specifically, higher MBR before IVB was correlated with lower FT after IVB.

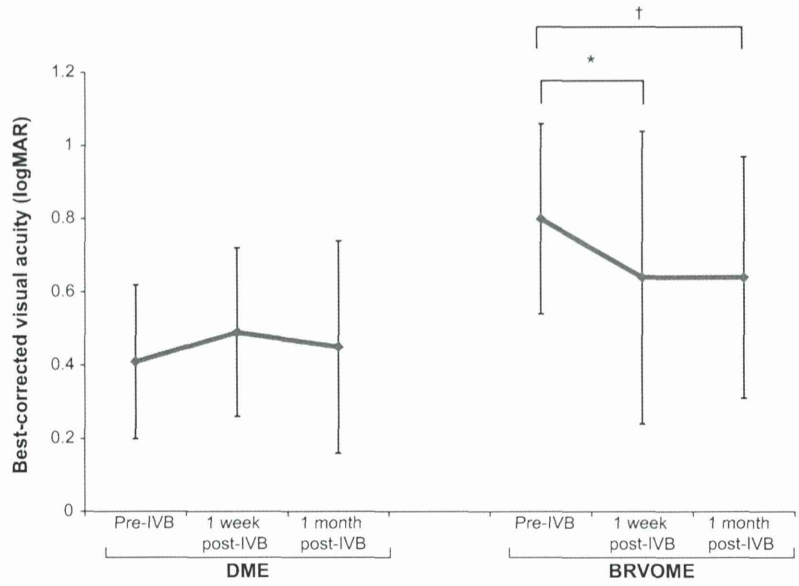

Figure 1 Best-corrected visual acuity before and after intravitreal injection of bevacizumab.
Notes: BCVA did not change significantly after 1 week or 1 month in the DME group (P=0.34) but did in the BRVOME group (P=0.049), with the most significant improvement being 1 week after IVB (P=0.03); Freidman test compared between three points pre-IVB, 1 week post-IVB, 1 month post-IVB; †P<0.05, Scheffe's paired comparison compares between groups, *P<0.05.
Abbreviations: BCVA, best-corrected visual acuity; BRVOME, branch retinal vein occlusion-associated macular edema; DME, diabetic macular edema; IVB, intravitreal bevacizumab; logMAR, logarithm of the minimum angle resolution.

There are no reports on the influence of IVB on intraocular microcirculation predating the current study. Our study, in which we analyzed the results of only a single injection, broadly agrees with existing reports showing that IVB leads to a significant improvement in FT and BCVA in patients with BRVOME.[5,9] Some earlier papers also found a similar improvement in patients with DME,[28–30] but our study contradicts such findings. The exact reason for this discrepancy is unclear, but it may be related to differences in injection times and follow-up periods, pre-IVB BCVA, differences in the demographics of the DME patients, or the small number of participants in this study. One of the most interesting findings of this study, that IVB reduces MBR in all regions of the eye in patients with DME, has not been previously reported. Previous reports on post-IVB ocular circulation used color Doppler imaging (CDI) and found that blood flow decreased after IVB in the ophthalmic artery, the posterior ciliary artery, and the central retinal artery.[12,31] These studies were unable to report on blood flow within the eye itself, however, as the intraocular vessels are too small to allow CDI to function. Access to LSFG was therefore a major advantage of this study since it allowed us to directly measure MBR in the retinal vessel, ONH, and choroid and confirm the reduction of ocular blood flow in eyes with DME. We also observed a decrease in choroidal MBR in the BRVOME group, most likely because, as shown in previous reports,[32,33] the choroid lacks an autoregulation system and is easily affected by exercise. Our findings for the choroid were based on measurements taken of the MBR in retinal regions lacking large vessels, in accord with established practice for LSFG measurement of the choroid.[34]

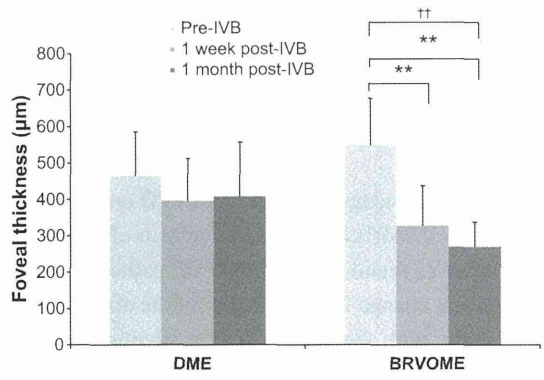

Figure 2 Foveal thickness before and after intravitreal injection of bevacizumab.
Notes: FT did not change significantly 1 week or 1 month after IVB in the DME group (P=0.20), but did in the BRVOME group (P<0.001). FT improved in patients with BRVOME both 1 week and 1 month after IVB (P=0.007 and P<0.001, respectively); Friedman test compared between three points pre-IVB, 1 week post-IVB, 1 month post-IVB; ††P<0.01; Scheffe's paired comparison compared between groups, **P<0.01.
Abbreviations: BRVOME, branch retinal vein occlusion-associated macular edema; DME, diabetic macular edema; FT, foveal thickness; IVB, intravitreal bevacizumab.

Another interesting finding of our study was that the lack of structural improvement in the DME patients may have been related to the decrease in MBR in the ONH observed before

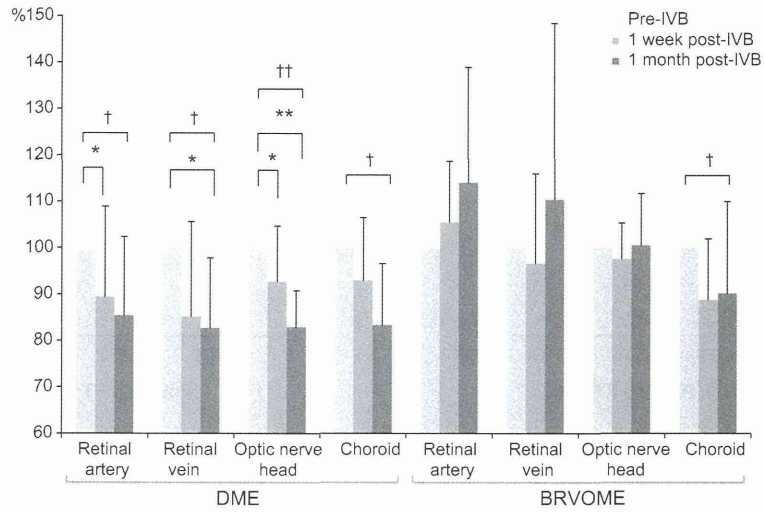

Figure 3 Mean blur rate in the retinal artery, retinal vein, optic nerve head, and choroid before and after intravitreal injection of bevacizumab.

Notes: In patients with DME, a comparison of MBR values before, 1 week after, and 1 month after IVB revealed significant changes in all measured regions (retinal artery, $P=0.02$; retinal vein, $P=0.04$; ONH, $P<0.001$; and choroid, $P=0.04$). MBR after 1 week fell significantly in the retinal artery by 10.6% ($P=0.03$) and in the ONH by 7.27% ($P=0.049$). MBR after 1 week also fell by 14.8% ($P=0.19$) in the retinal vein and by 6.97% ($P=0.15$) in the choroid, but these differences were not significant. MBR after 1 month fell significantly in the retinal vein by 17.3% ($P=0.049$) and in the ONH by 17.1% ($P<0.001$). MBR after 1 month also fell by 14.7% in the retinal artery ($P=0.08$) and 16.7% in the choroid ($P=0.06$), but these differences were not significant. In patients with BRVOME, a comparison of MBR values before, 1 week after, and 1 month after IVB revealed a significant change only in the choroid ($P=0.04$). Significant changes in MBR were not observed in the retinal artery ($P=0.09$), retinal vein ($P=0.33$), or the ONH ($P=0.50$). Significant changes in blood flow were not found after 1 week in any of the measured regions (retinal artery, $P=0.39$; retinal vein, $P=0.84$; ONH, $P=0.50$; and choroid, $P=0.09$). Furthermore, significant changes were not found in blood flow after 1 month in any of the measured regions (retinal artery, $P=0.10$; retinal vein, $P=0.67$; ONH, $P=0.84$; and choroid, $P=0.07$). Finally, significant changes were not found when comparing blood flow 1 week and 1 month after IVB in any of the regions (retinal artery, $P=0.73$; retinal vein, $P=0.33$; ONH, $P=0.84$; and choroid, $P=1.00$); Friedman test compared between points pre-IVB, 1 week post-IVB, 1 month post-IVB; $^{\dagger}P<0.05$, $^{\dagger\dagger}P<0.01$; Scheffe's paired comparison compares between groups, $^{*}P<0.05$, $^{**}P<0.01$.

Abbreviations: BRVOME, branch retinal vein occlusion-associated macular edema; DME, diabetic macular edema; IVB, intravitreal bevacizumab; MBR, mean blur rate; ONH, optic nerve head.

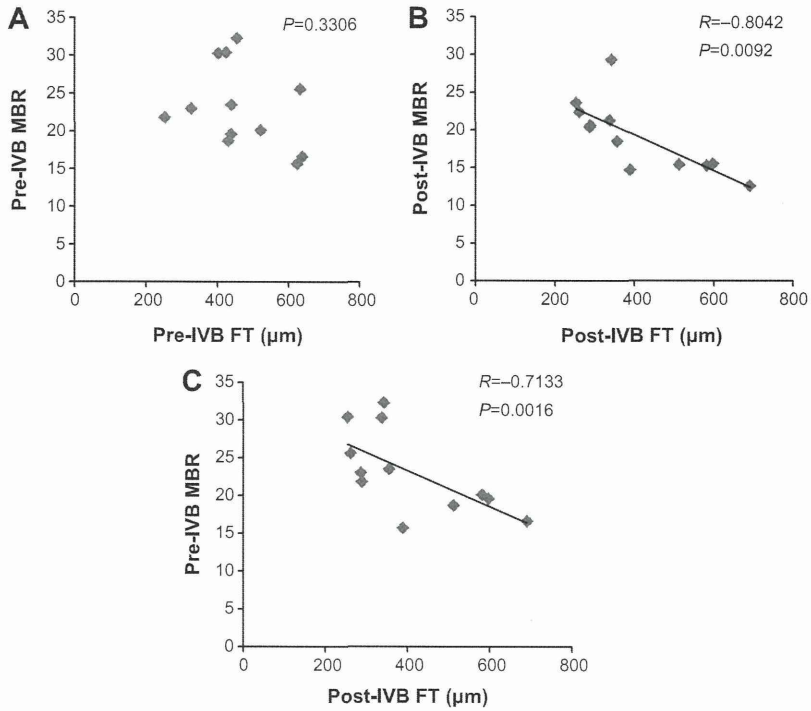

Figure 4 Relationship between foveal thickness and mean blur rate in eyes with diabetic macular edema.

Notes: Pre-IVB MBR was not correlated with pre-IVB FT ($P=0.33$) (**A**). However, post-IVB MBR was correlated with post-IVB FT ($R=-0.80$, $P=0.01$) (**B**). Furthermore, pre-IVB MBR was correlated with post-IVB FT ($R=-0.71$, $P=0.002$) (**C**). One MBR sample is represented by one pixel.

Abbreviations: FT, foveal thickness; IVB, intravitreal bevacizumab; MBR, mean blur rate.

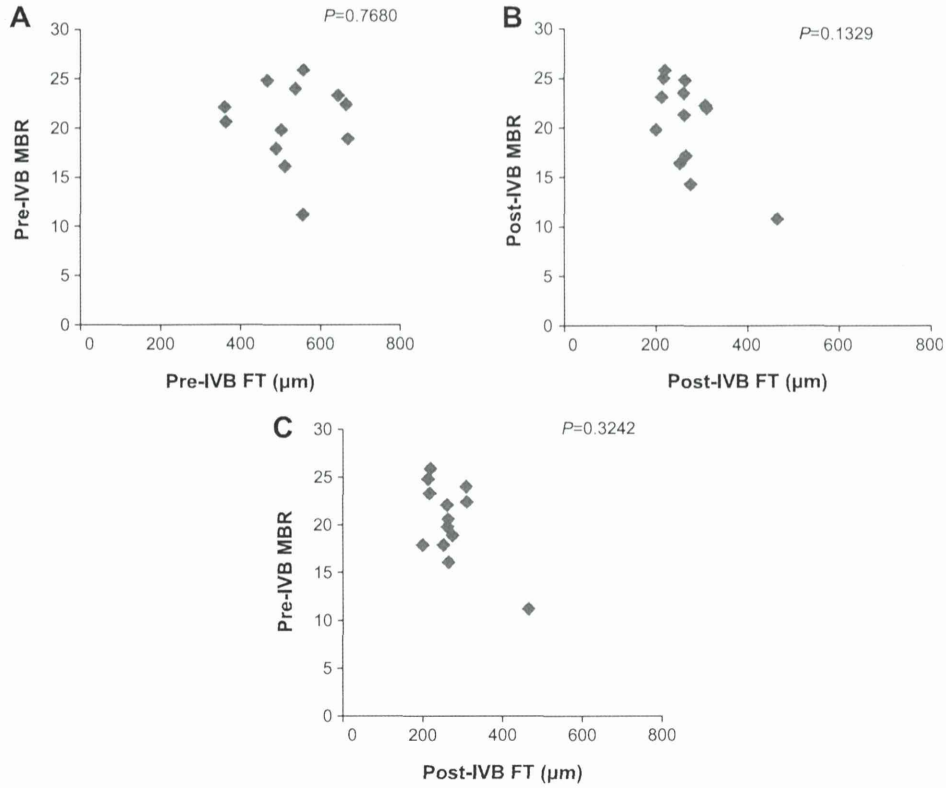

Figure 5 Relationship between foveal thickness and mean blur rate in eyes with branch retinal vein occlusion-associated macular edema.
Notes: Pre-IVB MBR was not correlated with pre-IVB FT (P=0.77) (**A**), nor was post-IVB MBR correlated with post-IVB FT (P=0.13) (**B**). In addition, pre-IVB MBR was not correlated with post-IVB FT (P=0.32) (**C**). One MBR sample is represented by one pixel.
Abbreviations: FT, foveal thickness; IVB, intravitreal bevacizumab; MBR, mean blur rate.

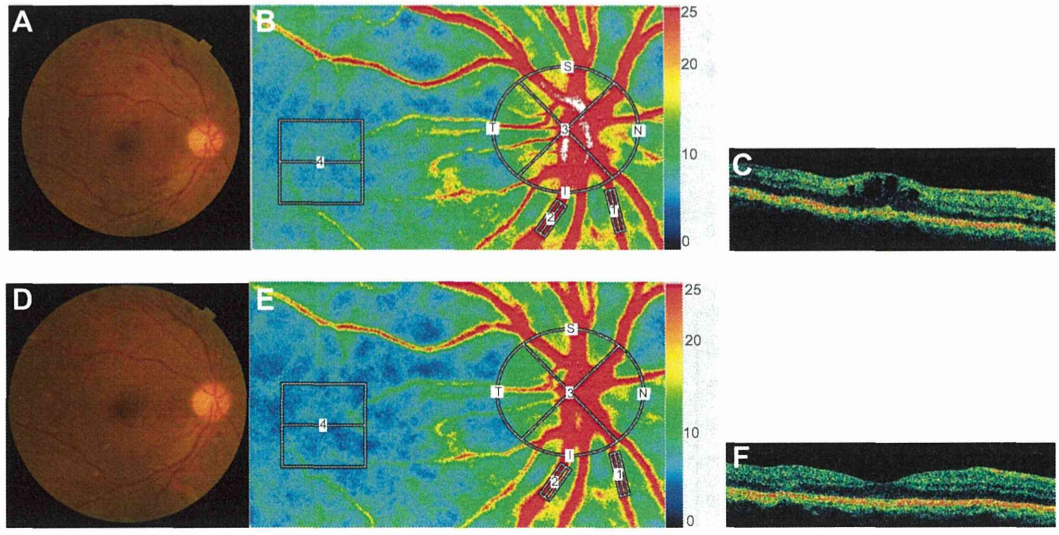

Figure 6 Representative eye with diabetic macular edema.
Notes: Images from a 59-year-old man with DME in his right eye; Fundus color photographs (**A** and **D**), color LSFG maps (**B** and **E**), and axial OCT images at fovea (**C** and **F**) are shown. Pre-IVB findings are above (**A**, **B**, and **C**) and findings 1 month after IVB are below (**D**, **E**, and **F**). In the color LSFG maps (**B** and **E**), the numbers 1 and 2 indicate the rectangular scanning areas for the retinal artery and vein, respectively; 3 and 4 indicate the circular and square scanning areas for the optic nerve head and choroid, respectively. Pre-IVB MBR was 30.1 in the retinal artery, 43.6 in the retinal vein, 31.0 in the optic nerve head, and 7.0 in the choroid. MBR 1 month after IVB was 22.6 (24.9% decrease) in the retinal artery, 30.3 (30.5% decrease) in the retinal vein, 24.2 (21.9% decrease) in the optic nerve head, and 5.8 (17.1% decrease) in the choroid. Decimal best-corrected visual acuity in the right eye was 0.3 before IVB and did not change 1 month after IVB. FT in the right eye was 425 μm before IVB and 272 μm 1 month after IVB.
Abbreviations: DME, diabetic macular edema; FT, foveal thickness; IVB, intravitreal bevacizumab; LSFG, laser speckle flowgraphy; MBR, mean blur rate; OCT, optical coherence tomography.

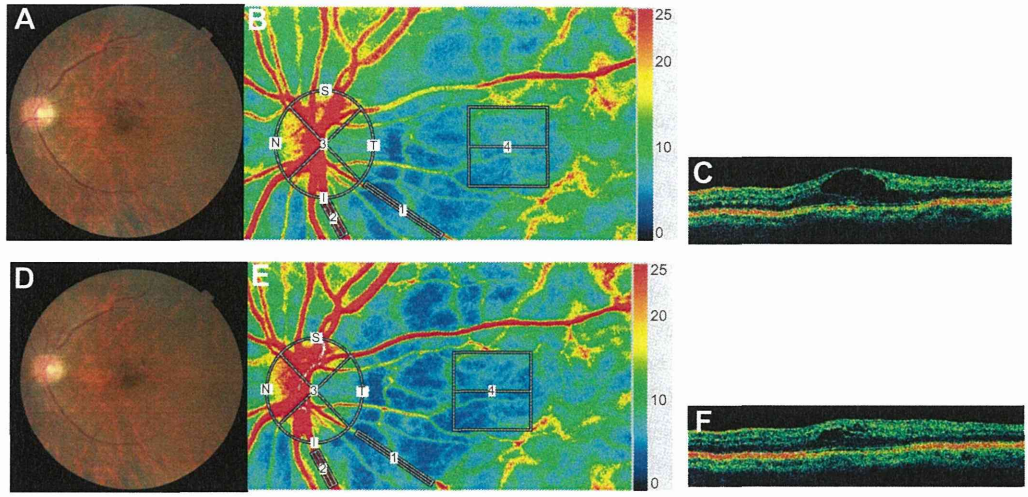

Figure 7 Representative eye with branch retinal vein occlusion-associated macular edema.
Notes: Images from a 65-year-old woman with BRVOME in her left eye. Fundus color photographs (**A** and **D**), color LSFG maps (**B** and **E**), and axial OCT images at fovea (**C** and **F**) are shown. Pre-IVB findings are above (**A**, **B**, and **C**) and findings 1 month after IVB are below (**D**, **E**, and **F**). In the color LSFG maps (**B** and **E**), the numbers 1 and 2 indicate the rectangular scanning areas for the retinal artery and vein, respectively; 3 and 4 indicate the circular and square scanning areas for the optic nerve head and choroid, respectively. Pre-IVB MBR was 15.9 in the retinal artery, 35.7 in the retinal vein, 23.5 in the optic nerve head, and 7.2 in the choroid. MBR 1 month after IVB was 14.0 (12.0% decrease) in the retinal artery, 33.4 (6.4% decrease) in the retinal vein, 26.0 (10.6% increase) in the optic nerve head, and 6.2 (13.9% decrease) in the choroid. Decimal best-corrected visual acuity in the right eye was 0.5 before IVB and did not change after 1 month. FT in the right eye was 364 μm before IVB and 264 μm 1 month after IVB.
Abbreviations: BRVOME, branch retinal vein occlusion-associated macular edema; FT, foveal thickness; IVB, intravitreal bevacizumab; LSFG, laser speckle flowgraphy; MBR, mean blur rate; OCT, optical coherence tomography.

IVB and 1 month after IVB. We observed no such association in the BRVO group. This is an interesting discrepancy that may be related to the pathogenesis of each type of macular edema. However, it should be noted that the characteristics of the two groups in our study did not match perfectly, differing in sex distribution and pre-IVB BCVA. From these results, however, we believe that it is fair to speculate that the effect of bevacizumab on intraocular tissues changes in the presence of systemic diseases such as diabetes. In our study, the eyes with DME probably experienced the effects of excessive VEGF over the entire retina, while the effects were limited to the obstructed retinal vein and its surrounding tissues in the eyes with BRVOME. The eyes with BRVOME even showed an increase in MBR after IVB, particularly in the artery, although we could not confirm the significance of the difference statistically. If such an increase occurs, it is likely to be part of retinal autoregulation, as a compensatory increase in arterial flow rate to maintain retinal circulation. We believe that this is because in eyes with BRVOME, the retinal vessels are less damaged than in eyes with DME. Most studies of DR have noted upregulation of inducible nitric oxide synthase,[35,36] with subsequent capillary degeneration, pericyte loss and permeability.[37,38] Though the status of ocular blood flow in DR is still the subject of debate,[39,40] CDI and laser Doppler flowmetry have revealed that the velocity of blood flow in the ophthalmic artery and choroidal blood flow both decrease in eyes with DR.[41,42] We believe that retinal autoregulation may be impaired in patients with DR and, furthermore, that the additional decrease in retinal circulation caused by IVB leads to an acceleration of the original chronic ischemia in eyes with DR, explaining the appearance of macular ischemia after IVB in patients with underlying diseases such as diabetes.[14,15] Caution is therefore indicated when administering anti-VEGF antibodies, including bevacizumab, to DR patients. Even in eyes with BRVOME, although IVB can lead to a temporary reduction of the condition, we cannot exclude the possibility that IVB may also cause an adverse reduction in ocular circulation, particularly in the choroid. Thus, follow-up care in patients undergoing IVB should include LSFG examinations of ocular blood circulation, in addition to standard examinations of retinal structure and function.

It is difficult to make a prognosis on the structure and function of eyes with macular edema after IVB, especially for eyes with DME. Several biochemical mechanisms may contribute to the vascular disruptions that characterize DR and DME.[43] The pathogenesis of DME is still unclear but is thought to have several clinical aspects, including inflammation, disruption of the capillary barrier, and dysfunction of the retinal pigment epithelium. In our study, pre-IVB MBR in the ONH was significantly correlated with post-IVB FT of eyes with DME, a result indicating that IVB is not effective for patients with DME and low MBR. We believe that MBR of the ONH can be regarded as a clinically reliable preintervential parameter, and that the predictive value of pre-IVB

MBR may prove to be of importance, especially because LSFG measurements of MBR in the ONH have been reported to be highly reproducible.[44] In fact, IVB is not always fully effective in reducing DME, and the pathogenesis of DME may include an IVB-sensitive mechanism related to vascular hyperpermeability (elevated MBR) and a non-IVB-sensitive mechanism, possibly related to impairment of the retinal pigment epithelium. Thus, we believe that the pathogenesis of DME may depend not only on VEGF, but also on other mechanisms suppressed by corticosteroids, as intravitreal injection of triamcinolone acetonide showed better results than IVB in reducing DME and improving BCVA.[45] There are also reports showing that BRVOME is closely related to intraocular levels of cytokines such as macrophage inflammatory protein-1β and interleukin-6 but not of VEGF.[46,47]

Our study was limited by a small sample size, the exclusion of types of macular edema besides BRVOME and DME, the restriction of the data to 1 month after IVB, and by the fact that characteristics were not matched between the two groups. We were also not able to find more than a weak connection between visual acuity and MBR. Nevertheless, we believe our results show that in eyes with BRVOME, IVB is currently a good choice to aid in recovery of FT and visual acuity, without a concomitant decrease in retinal blood flow, at least until such time as other antibodies are ready for clinical use. Furthermore, we are the first to report that pre-IVB MBR is significantly correlated with post-IVB FT in patients with DME, indicating the possible existence of VEGF- and MBR-dependent DME.

In conclusion, we found that in patients with BRVOME, there was no significant change in MBR in the retinal artery, retinal vein, or ONH. In patients with DME, MBR in all measured areas decreased significantly. Furthermore, pre-IVB MBR was significantly correlated with post-IVB FT in patients with DME, but there was no such correlation in patients with BRVOME. Higher pre-IVB MBR in these patients was an indicator of lower post-IVB FT. Measuring MBR with LSFG, therefore, has the potential to serve as a noninvasive and objective biomarker to help clinicians determine the value of IVB treatments for patients with DME. The focus of further investigation should be a determination of MBR relationship to the mechanism behind IVB-induced reduction of DME and BRVOME.

Author contributions

HK and TN were responsible for the design and conduct of the study. FN, HK, NA, KO, YS, and MY were responsible for the collection, management, analysis, and interpretation of the data. HK and TN were responsible for the preparation, review, and approval of the manuscript. All authors contributed toward data analysis, drafting and revising the paper and agree to be accountable for all aspects of the work.

Disclosure

This paper was partially presented at the 27th Annual Meeting of the Japanese Society for Ocular Circulation, Kobe, Japan, 2010. This paper was supported in part by JST grant, JSPS KAKENHI Grant-in-Aid for Scientific Research (B) (T.N. 26293372), for Scientific Research (C) (H.K. 26462629), and for Exploratory Research (T.N. 26670751). The authors report no conflicts of interest in this work.

References

1. Argon laser photocoagulation for macular edema in branch vein occlusion. The Branch Vein Occlusion Study Group. *Am J Ophthalmol.* 1984; 98(3):271–282.
2. Ferris FL 3rd, Patz A. Macular edema: a major complication of diabetic retinopathy. *Trans New Orleans Acad Ophthalmol.* 1983;31: 307–316.
3. Gutman FA, Zegarra H. Macular edema secondary to occlusion of the retinal veins. *Surv Ophthalmol.* 1984;28 Suppl:462–470.
4. Sigelman J. Diabetic macular edema in juvenile- and adult-onset diabetes. *Am J Ophthalmol.* 1980;90(3):287–296.
5. Yilmaz T, Cordero-Coma M. Use of bevacizumab for macular edema secondary to branch retinal vein occlusion: a systematic review. *Graefes Arch Clin Exp Ophthalmol.* 2012;250(6):787–793.
6. Kang HM, Chung EJ, Kim YM, Koh HJ. Spectral-domain optical coherence tomography (SD-OCT) patterns and response to intravitreal bevacizumab therapy in macular edema associated with branch retinal vein occlusion. *Graefes Arch Clin Exp Ophthalmol.* 2013;251(2): 501–508.
7. Shimura M, Yasuda K, Yasuda M, Nakazawa T. Visual outcome after intravitreal bevacizumab depends on the optical coherence tomographic patterns of patients with diffuse diabetic macular edema. *Retina.* 2013; 33(4):740–747.
8. Solaiman KA, Diab MM, Dabour SA. Repeated intravitreal bevacizumab injection with and without macular grid photocoagulation for treatment of diffuse diabetic macular edema. *Retina.* 2013;33(8):1623–1629.
9. Siegel RA, Dreznik A, Mimouni K, Bor E, Weinberger D, Bourla DH. Intravitreal bevacizumab treatment for macular edema due to branch retinal vein occlusion in a clinical setting. *Curr Eye Res.* 2012;37(9): 823–829.
10. Hanada N, Iijima H, Sakurada Y, Imasawa M. Recurrence of macular edema associated with branch retinal vein occlusion after intravitreal bevacizumab. *Jpn J Ophthalmol.* 2012;56(2):165–174.
11. Gulkilik G, Taskapili M, Kocabora S, Muftuoglu G, Demirci G. Intravitreal bevacizumab for persistent macular edema with proliferative diabetic retinopathy. *Int Ophthalmol.* 2010;30(6):697–702.
12. Hosseini H, Lotfi M, Esfahani MH, et al. Effect of intravitreal bevacizumab on retrobulbar blood flow in injected and uninjected fellow eyes of patients with neovascular age-related macular degeneration. *Retina.* 2012;32(5):967–971.
13. Matsuyama K, Ogata N, Matsuoka M, Wada M, Takahashi K, Nishimura T. Plasma levels of vascular endothelial growth factor and pigment epithelium-derived factor before and after intravitreal injection of bevacizumab. *Br J Ophthalmol.* 2010;94(9):1215–1218.
14. Shimura M, Yasuda K. Macular ischaemia after intravitreal bevacizumab injection in patients with central retinal vein occlusion and a history of diabetes and vascular disease. *Br J Ophthalmol.* 2010;94(3): 381–383.
15. Huang ZL, Lin KH, Lee YC, Sheu MM, Tsai RK. Acute vision loss after intravitreal injection of bevacizumab (avastin) associated with ocular ischemic syndrome. *Ophthalmologica.* 2010;224(2):86–89.

16. Yoshida Y, Sugiyama T, Utsunomiya K, Ogura Y, Ikeda T. A pilot study for the effects of donepezil therapy on cerebral and optic nerve head blood flow, visual field defect in normal-tension glaucoma. *J Ocul Pharmacol Ther*. 2010;26(2):187–192.
17. Sugiyama T, Kojima S, Ishida O, Ikeda T. Changes in optic nerve head blood flow induced by the combined therapy of latanoprost and beta blockers. *Acta Ophthalmol*. 2009;87(7):797–800.
18. Takahashi H, Sugiyama T, Tokushige H, et al. Comparison of CCD-equipped laser speckle flowgraphy with hydrogen gas clearance method in the measurement of optic nerve head microcirculation in rabbits. *Exp Eye Res*. 2013;108:10–15.
19. Wang L, Cull GA, Piper C, Burgoyne CF, Fortune B. Anterior and posterior optic nerve head blood flow in nonhuman primate experimental glaucoma model measured by laser speckle imaging technique and microsphere method. *Invest Ophthalmol Vis Sci*. 2012;53(13):8303–8309.
20. Nagahara M, Tamaki Y, Araie M, Fujii H. Real-time blood velocity measurements in human retinal vein using the laser speckle phenomenon. *Jpn J Ophthalmol*. 1999;43(3):186–195.
21. Nagahara M, Tamaki Y, Tomidokoro A, Araie M. In vivo measurement of blood velocity in human major retinal vessels using the laser speckle method. *Invest Ophthalmol Vis Sci*. 2011;52(1):87–92.
22. Aizawa N, Kunikata H, Yokoyama Y, Nakazawa T. Correlation between optic disc microcirculation in glaucoma measured with laser speckle flowgraphy and fluorescein angiography, and the correlation with mean deviation. *Clin Experiment Ophthalmol*. 2014;42(3):293–294.
23. Yokoyama Y, Aizawa N, Chiba N, et al. Significant correlations between optic nerve head microcirculation and visual field defects and nerve fiber layer loss in glaucoma patients with myopic glaucomatous disk. *Clin Ophthalmol*. 2011;5:1721–1727.
24. Chiba N, Omodaka K, Yokoyama Y, et al. Association between optic nerve blood flow and objective examinations in glaucoma patients with generalized enlargement disc type. *Clin Ophthalmol*. 2011;5:1549–1556.
25. Sugiyama T, Araie M, Riva CE, Schmetterer L, Orgul S. Use of laser speckle flowgraphy in ocular blood flow research. *Acta Ophthalmol*. 2010;88(7):723–729.
26. Fabick MM. Ethical considerations for research on human subjects. *Plast Surg Nurs*. 1995;15(4):225–227, 231.
27. Enserink M. Bioethics. Helsinki's new clinical rules: fewer placebos, more disclosure. *Science*. 2000;290(5491):418–419.
28. Forte R, Cennamo GL, Finelli M, et al. Intravitreal bevacizumab vs intravitreal triamcinolone combined with macular laser grid for diffuse diabetic macular oedema. *Eye (Lond)*. 2010;24(8):1325–1330.
29. Arevalo JF, Sanchez JG, Wu L, et al; Pan-American Collaborative Retina Study Group. Primary intravitreal bevacizumab for diffuse diabetic macular edema: the Pan-American Collaborative Retina Study Group at 24 months. *Ophthalmology*. 2009;116(8):1488–1497, 1497.e1.
30. Paccola L, Costa RA, Folgosa MS, Barbosa JC, Scott IU, Jorge R. Intravitreal triamcinolone versus bevacizumab for treatment of refractory diabetic macular oedema (IBEME study). *Br J Ophthalmol*. 2008;92(1):76–80.
31. Bonnin P, Pournaras JA, Lazrak Z, et al. Ultrasound assessment of short-term ocular vascular effects of intravitreal injection of bevacizumab (Avastin®) in neovascular age-related macular degeneration. *Acta Ophthalmol*. 2010;88(6):641–645.
32. Okuno T, Sugiyama T, Kohyama M, Kojima S, Oku H, Ikeda T. Ocular blood flow changes after dynamic exercise in humans. *Eye (Lond)*. 2006;20(7):796–800.
33. Shiga Y, Shimura M, Asano T, Tsuda S, Yokoyama Y, Aizawa N, Omodaka K, et al. The influence of posture change on ocular blood flow in normal subjects, measured by laser speckle flowgraphy. *Curr Eye Res*. 2013;38(6):691–698.
34. Isono H, Kishi S, Kimura Y, Hagiwara N, Konishi N, Fujii H. Observation of choroidal circulation using index of erythrocytic velocity. *Arch Ophthalmol*. 2003;121(2):225–231.
35. Carmo A, Cunha-Vaz JG, Carvalho AP, Lopes MC. Nitric oxide synthase activity in retinas from non-insulin-dependent diabetic Goto-Kakizaki rats: correlation with blood-retinal barrier permeability. *Nitric Oxide*. 2000;4(6):590–596.
36. Abu El-Asrar AM, Desmet S, Meersschaert A, Dralands L, Missotten L, Geboes K. Expression of the inducible isoform of nitric oxide synthase in the retinas of human subjects with diabetes mellitus. *Am J Ophthalmol*. 2001;132(4):551–556.
37. Zheng L, Du Y, Miller C, et al. Critical role of inducible nitric oxide synthase in degeneration of retinal capillaries in mice with streptozotocin-induced diabetes. *Diabetologia*. 2007;50(9):1987–1996.
38. Leal EC, Manivannan A, Hosoya K, et al. Inducible nitric oxide synthase isoform is a key mediator of leukostasis and blood-retinal barrier breakdown in diabetic retinopathy. *Invest Ophthalmol Vis Sci*. 2007;48(11):5257–5265.
39. Grunwald JE, Brucker AJ, Grunwald SE, Riva CE. Retinal hemodynamics in proliferative diabetic retinopathy. A laser Doppler velocimetry study. *Invest Ophthalmol Vis Sci*. 1993;34(1):66–71.
40. Patel V, Rassam S, Newsom R, Wiek J, Kohner E. Retinal blood flow in diabetic retinopathy. *BMJ*. 1992;305(6855):678–683.
41. Gracner T. Ocular blood flow velocity determined by color Doppler imaging in diabetic retinopathy. *Ophthalmologica*. 2004;218(4):237–242.
42. Nagaoka T, Kitaya N, Sugawara R, et al. Alteration of choroidal circulation in the foveal region in patients with type 2 diabetes. *Br J Ophthalmol*. 2004;88(8):1060–1063.
43. Ciulla TA, Amador AG, Zinman B. Diabetic retinopathy and diabetic macular edema: pathophysiology, screening, and novel therapies. *Diabetes Care*. 2003;26(9):2653–2664.
44. Aizawa N, Yokoyama Y, Chiba N, et al. Reproducibility of retinal circulation measurements obtained using laser speckle flowgraphy-NAVI in patients with glaucoma. *Clin Ophthalmol*. 2011;5:1171–1176.
45. Shimura M, Nakazawa T, Yasuda K, et al. Comparative therapy evaluation of intravitreal bevacizumab and triamcinolone acetonide on persistent diffuse diabetic macular edema. *Am J Ophthalmol*. 2008;145(5):854–861.
46. Shimura M, Nakazawa T, Yasuda K, Kunikata H, Shiono T, Nishida K. Visual prognosis and vitreous cytokine levels after arteriovenous sheathotomy in branch retinal vein occlusion associated with macular oedema. *Acta Ophthalmol*. 2008;86(4):377–384.
47. Kunikata H, Shimura M, Nakazawa T, et al. Chemokines in aqueous humour before and after intravitreal triamcinolone acetonide in eyes with macular oedema associated with branch retinal vein occlusion. *Acta Ophthalmol*. 2012;90(2):162–167.

Journal of Neuroscience Research

Journal of Neuroscience Research 92:1134–1142 (2014)

Critical Neuroprotective Roles of Heme Oxygenase-1 Induction Against Axonal Injury-Induced Retinal Ganglion Cell Death

Noriko Himori, Kazuichi Maruyama, Kotaro Yamamoto, Masayuki Yasuda, Morin Ryu, Kazuko Omodaka, Yukihiro Shiga, Yuji Tanaka, and Toru Nakazawa*

Department of Ophthalmology, Tohoku University Graduate School of Medicine, Miyagi, Japan

Although axonal damage induces significant retinal ganglion cell (RGC) death, small numbers of RGCs are able to survive up to 7 days after optic nerve crush (NC) injury. To develop new treatments, we set out to identify patterns of change in the gene expression of axonal damage-resistant RGCs. To compensate for the low density of RGCs in the retina, we performed retrograde labeling of these cells with 4Di-10ASP in adult mice and 7 days after NC purified the RGCs with fluorescence-activated cell sorting. Gene expression in the cells was determined with a microarray, and the expression of *Ho-1* was determined with quantitative PCR (qPCR). Changes in protein expression were assessed with immunohistochemistry and immunoblotting. Additionally, the density of Fluoro-gold-labeled RGCs was counted in retinas from mice pretreated with CoPP, a potent HO-1 inducer. The microarray and qPCR analyses showed increased expression of *Ho-1* in the post-NC RGCs. Immunohistochemistry also showed that HO-1-positive cells were present in the ganglion cell layer (GCL), and cell counting showed that the proportion of HO-1-positive cells in the GCL rose significantly after NC. Seven days after NC, the number of RGCs in the CoPP-treated mice was significantly higher than in the control mice. Combined pretreatment with SnPP, an HO-1 inhibitor, suppressed the neuroprotective effect of CoPP. These results reflect changes in HO-1 activity to RGCs that are a key part of RGC survival. Upregulation of HO-1 signaling may therefore be a novel therapeutic strategy for glaucoma.

Key words: heme oxygenase-1; retinal ganglion cell; glaucoma; neuroprotection

According to global surveys (Quigley, 1996), glaucoma is the second most common cause of blindness, after cataracts. It is the foremost type of optic neuropathy, in which the ultimate cause of vision loss is thought to be retinal ganglion cell (RGC) apoptosis (Yücel et al., 2003). The RGCs are the only neurons connected to the brain by the optic nerve, and a significant dying off of these cells is characteristic of glaucoma. There are a variety of mechanisms causing RGC death, including oxidative stress (Izzotti et al., 2006; Ferreira et al., 2010; Yuki et al., 2011), excitatory amino acids such as glutamate (Sullivan et al., 2006; Harada et al., 2007), endoplasmic reticulum stress (Uchibayashi et al., 2011), and nitric oxide (Neufeld et al., 1999). Therefore, neuroprotection of the RGCs has recently drawn attention as a new approach to glaucoma therapy.

Several studies have provided evidence that oxidative stress and the related damage contribute to glaucomatous degeneration of the RGCs (Tezel, 2006). Oxidative-stress-induced change can either cause RGC damage and death directly or trigger downstream effects (Tezel, 2006). Although an elevated intraocular pressure (higher than 21 mmHg) is the greatest risk factor for primary open-angle glaucoma, normal-tension glaucoma (NTG), the most common type worldwide and the prevalent type in Asia (Iwase et al. 2004), occurs in eyes with normal intraocular pressure (10–21 mmHg). The pathogenesis of RGC death in NTG has yet to be elucidated, even though the vulnerability of the RGCs is well known. Nerve crush (NC) is a commonly used model of axonal injury that provides insight into the mechanisms involved in the death of the RGCs. It involves applying a precise, short-term,

Contract grant sponsor: Ministry of Education, Science and Technology of Japan; Contract grant number: 23592613 (to K.M). This paper was supported in part by JSPS KAKENHI Grant-in-Aid for Scientific Research (B) (T.N. 26293372), for Exploratory Research (T.N. 26670751), and for young scientists (N.H. 26861434).

*Correspondence to: Toru Nakazawa, MD, PhD, Tohoku University Graduate School of Medicine, Department of Ophthalmology, 1-1 Seiryo, Aoba, Sendai, Miyagi 980-8574, Japan.
E-mail: ntoru@fa2.so-net.ne.jp

Received 17 February 2014; Revised 10 March 2014; Accepted 1 April 2014

Published online 5 May 2014 in Wiley Online Library (wileyonlinelibrary.com). DOI: 10.1002/jnr.23398

synchronous insult to the axons, which results in secondary RGC apoptotic cell death resembling glaucoma.

Several studies have used microarrays for genome-wide analysis of the retina in models of glaucoma and in DBA/2J mice (Steele et al., 2006; Panagis et al., 2010). The RGCs represent only a small percentage of the total cell population in the retina, however, and microarray analysis can miss many responses specific to the RGCs. To supplement the broad analysis provided by microarray, therefore, we also used fluorescence-activated cell sorting (FACS) to isolate the RGCs from other cells in the retina.

Heme oxygenase (HO), the rate-limiting enzyme in heme catabolism, catalyzes the degradation of heme to biliverdin, with the concurrent release of iron and carbon monoxide. Three isoforms have been identified, HO-1, HO-2, and HO-3 (Mancuso, 2004). HO-1 (also known as *heat-shock protein 32*) is induced by certain cellular stress conditions, including heat shock (Shibahara et al., 1987), oxidative damage (Keyse and Tyrrell, 1989), and ischemia–reperfusion injury (Takeda et al., 1994). The use of gene transfer or drugs to induce HO-1 has been shown to inhibit apoptosis and to provide cellular protection after injury (Li Volti et al., 2007; Lai et al., 2008; Peng et al., 2008, 2011). Recently, such newly proposed neuroprotective strategies have become the subject of investigation as new goals for glaucoma therapy (Lebrun-Julien and Di Polo, 2008; Weber et al., 2008). Changes during the early stages of glaucoma may increase the vulnerability of the RGCs, which might explain the progression of vision loss in patients despite IOP-lowering therapy in open angle glaucoma or in non-IOP-dependent types of glaucoma such as NTG. Insights into the mechanisms of axonal-damage-induced RGC death are therefore urgently needed to aid in the development of new neuroprotective treatment strategies for patients with glaucoma.

MATERIALS AND METHODS

Animals

Adult, 10-12-week-old male C57BL/B6 mice (SLC, Shizuoka, Japan), housed in covered cages, were maintained and handled in accordance with the guidelines of the ARVO Statement for the Use of Animals in Ophthalmic and Vision Research and the guidelines from the declaration of Helsinki and the Guiding Principles in the Care and Use of Animals. All experimental procedures described in the present study were approved by the Ethics Committee for Animal Experiments at Tohoku University Graduate School of Medicine, and were performed according to the National Institutes of Health *Guidelines for the care and use of laboratory animals.*

Surgery

Retrograde labeling was performed according to established procedures (Ryu et al., 2012; Shanab et al., 2012). Briefly, the mice were anesthetized with a ketamine/xylazine mixture. The RGCs were retrogradely labeled with a fluorescent tracer, Fluoro-Gold (FG; Fluorochrome, Englewood, CO), or carbocyanine dye N-4-[4-didecylaminostryryl]-N-methyl-pyridinium iodide (4Di-10ASP; Molecular Probes, Eugene, OR). Either 3% 4Di-10ASP in dimethylformamide or 1 μl of 2% aqueous FG in 1% dimethylsulfoxide (DMSO) was injected into the superior colliculus with a 32-G needle. Seven days after FG labeling, an NC procedure was performed in the animals' right eyes.

Seven days after NC, the mice were sacrificed, and their complete retinas were placed on glass slides with the ganglion cell layer facing upward. RGC density was determined by counting tracer-labeled RGCs in 12 distinct areas under a microscope as previously described (Himori et al., 2013).

RGC Purification and Quantitative RT-PCR (qPCR)

The 4Di-10ASP-labeled RGCs were purified according to established procedures (Himori et al., 2013). Briefly, the 4Di-10ASP-labeled mice were euthanized 7 days after NC. The retinas were rapidly dissected, incubated in a digestion solution containing papain (10 U/ml; Worthington, Lakewood, NJ) and L-cysteine (0.3 mg/ml; Sigma, St. Louis, MO) in HBSS (37°C for 15 min; CO_2 incubator), rinsed twice in HBSS, and then triturated to create a single-cell suspension. The dissociated cells were promptly sorted using a FACS Aria II (Becton-Dickinson, San Jose, CA). The 4Di-10ASP-labeled RGCs were detected with a 585/42 filter. The cells were sorted directly into 350 μl of buffer RLT Plus (Qiagen, Valencia, CA) with 1% β-mercaptoethanol, frozen immediately, and stored at −80°C until further use. Samples of the post-NC RGCs and non-NC controls each contained 6,000 RGCs. Total RNA was extracted from FACS-purified RGCs by using an RNeasy Micro Kit (Qiagen) according to the manufacturer's protocol. The RNA was then concentrated using RNeasy MinElute Spin columns (Qiagen), and first-strand cDNA synthesis was performed with the SuperScript III First Strand Synthesis SuperMix for qRT-PCR (Invitrogen, Carlsbad, CA). Taqman Fast Universal PCR master mix (4352042; Applied Biosystems, Foster City, CA) was used for qPCR to quantify mRNA levels by using commercially available Taqman probes for *Ho-1* (Mm00516007_m1) and *Gapdh* (Mm99999915_g1). Relative gene expression levels were calculated by using the ΔΔCt method. The mRNA levels were normalized to *Gapdh* as an internal control.

DNA Microarray Analysis

Isolation of RGCs was performed as described above. Each sample contained ~100,000 RGCs, pooled from four to six individually sorted retinas, and yielded 50 ng of total RNA, which is enough for microarray analysis (Kurabo Industries, Osaka, Japan). We analyzed mRNA expression using GenopalR ROSM-JX chips (Mitsubishi Rayon, Tokyo, Japan) equipped with 219 oligonucleotide DNA probes in hollow plastic fibers specially designed to detect mouse mRNA sequences. Hybridization signals were analyzed using a DNA chip analyzer according to the manufacturer's instructions. DNA chip data were compared for analysis by Kurabo custom analysis services (Kurabo). Increases more than twofold were regarded as significant. The gene list is given in Table 1.

Immunohistochemistry

Immunohistochemistry was performed according to our previous publications (Nakazawa et al., 2006, 2007). The eyes

TABLE 1. Genes

Accession No.	Gene symbol	Gene description	NC−	NC+	Ratio
NM_015760.3	Nox4	NADPH oxidase 4 (Nox4)	12	98	8.30
NM_009663.1	Alox5ap	Arachidonate 5-lipoxygenase activating protein (Alox5ap)	43	332	7.68
NM_009155.3	Sepp1	Selenoprotein P, plasma, 1 (Sepp1)	212	1,399	6.60
NM_008871.1	Serpine1	Serine (or cysteine) peptidase inhibitor, clade E, member 1 (Serpine1)	101	653	6.49
NM_001037859.2	Csf1r	Colony- stimulating factor 1 receptor (Csf1r)	1105	7,041	6.37
NM_010907.1	Nfkbia	Nuclear factor of kappa light polypeptide gene enhancer in B-cells inhibitor, alpha (Nfkbia)	339	1,974	5.82
NM_009463.2	Ucp1	Uncoupling protein 1 (mitochondrial, proton carrier) (Ucp1)	12	62	5.04
NM_009740.1	Bcl10	B-cell leukemia/lymphoma 10 (Bcl10)	26	132	5.00
NM_010554.4	Il1a	Interleukin 1 alpha (Il1a)	133	610	4.60
NM_001009935.2	Txnip	Thioredoxin interacting protein (Txnip)	212	969	4.57
NM_019823.3	Cyp2d22	Cytochrome P450, family 2, subfamily d, polypeptide 22 (Cyp2d22)	132	556	4.22
NM_008185.2	Gstt1	Glutathione S-transferase, theta 1 (Gstt1)	234	945	4.04
NM_010442.1	Hmox1	Heme oxygenase (decycling) 1 (Hmox1)	329	1,074	3.27
NM_024264.4	Cyp27a1	Cytochrome P450, family 27, subfamily a, polypeptide 1 (Cyp27a1)	104	335	3.21
NM_008493.3	Lep	Leptin (Lep)	7	23	3.14
NM_008509.2	Lpl	Lipoprotein lipase (Lpl)	212	663	3.12
NM_001044384.1	Timp1	Tissue inhibitor of metalloproteinase 1 (Timp1)	27	76	2.84
NM_010361.2	Gstt2	Glutathione S-transferase, theta 2 (Gstt2)	47	132	2.79
NM_133994.3	Gstt3	Glutathione S-transferase, theta 3 (Gstt3)	64	169	2.64
NM_009744.3	Bcl6	B-cell leukemia/lymphoma 6 (Bcl6)	124	309	2.50
NM_008116.2	Ggt1	Gamma-glutamyltransferase 1 (Ggt1)	36	90	2.49
NM_011671.4	Ucp2	Uncoupling protein 2 (mitochondrial, proton carrier) (Ucp2)	5	12	2.31
NM_029555.2	Gstk1	Glutathione S-transferase kappa 1 (Gstk1)	91	210	2.30
NM_013602.2	Mt1	Metallothionein 1 (Mt1)	11,218	25,656	2.29
NM_010358.4	Gstm1	Glutathione S-transferase, mu 1 (Gstm1)	457	1,044	2.29
NM_008184.3	Gstm6	Glutathione S-transferase, mu 6 (Gstm6)	37	83	2.24
NM_011480.3	Srebf1	Sterol regulatory element binding transcription factor 1 (Srebf1)	518	1,141	2.20

were enucleated as described in the histological analysis section, fixed in 4% paraformaldehyde overnight at 4°C, immersed in a 20% sucrose solution, and embedded in an optimal cutting temperature compound (Sakura Finetechnical, Tokyo, Japan). Ten-micrometer-thick cryosections were mounted on the slides and incubated with blocking buffer (10% goat serum, 0.5% gelatin, 3% BSA, and 0.2% Tween 20 in PBS). Next, they were incubated with rabbit polyclonal anti-HO-1 antibody (1:200; Enzo Life Sciences, Farmingdale, NY) and mouse monoclonal anti-C38 antibody (graciously donated by T. Wakabayashi; Wakabayashi et al., 2010) overnight at 4°C. The sections were incubated with Alexa 488 secondary antibody (1:200; Invitrogen) for 1 hr. Photographs of the retina were taken in areas 500 μm and 1,000 μm from the center of the optic nerve using fluorescence illumination (Axiovert-200; Carl Zeiss, Jena, Germany). Cell counts were performed as described previously (Nakazawa et al., 2008). Briefly, a blind count was performed of immunopositive cells colocalized with DAPI-stained nuclei from four sections of a single eye's ganglion cell layer (GCL). The numbers were then averaged.

Experimental Protocol

Injections were prepared as follows: cobalt protoporphyrin IX (CoPP; Frontier Scientific, Logan, UT) was first dissolved in 0.1 N NaOH and further diluted to a final concentration of 0.02 N with PBS. Tin protoporphyrin (SnPP; Frontier Scientific) was dissolved in equal amounts of PBS and 0.1 N NaOH. The mice received intraperitoneal (IP) injections of CoPP (10 μmol/kg body weight) every 24 hr before NC for 3 days and after NC for 6 more days. IP injection of SnPP (10 μmol/kg body weight), when performed, was simultaneous with injection of CoPP. We then examined the number of RGCs 7 days after NC as described above.

Immunoblot Analysis

Three days after the administration of CoPP, the retinas were isolated and placed into a lysis buffer (Thermo Fisher Scientific, Waltham, MA) containing a 1% protease inhibitor cocktail (Sigma) and a 1% phosphatase inhibitor cocktail (Sigma). Cell lysates were clarified by centrifugation at 15,000*g* at 4°C for 20 min. Each sample was separated with SDS-PAGE and electroblotted onto a polyvinylidene fluoride (PVDF) membrane (Millipore, Bedford, MA). After nonspecific binding had been blocked with 4% BlockAce (Yukijirushi, Sapporo, Japan), the membranes were incubated at 4°C overnight with a rabbit polyclonal antibody against HO-1 (1:1,000; Enzo) or β-actin (1:5,000; Sigma). The membranes were then incubated with a horseradish peroxidase-conjugated anti-mouse or anti-rabbit immunoglobulin secondary antibody for 1 hr. The signals were visualized with chemiluminescence (ECL blotting analysis system; Amersham, Arlington Heights, IL), measured in Image Lab statistical software (Bio-Rad, Hercules, CA), and normalized to β-actin.

Statistical Analysis

All data are expressed as mean &plunmn; SD. The values were processed for statistical analysis (Mann-Whitney U test), followed by a two-tailed Student's *t*-test. Comparisons between

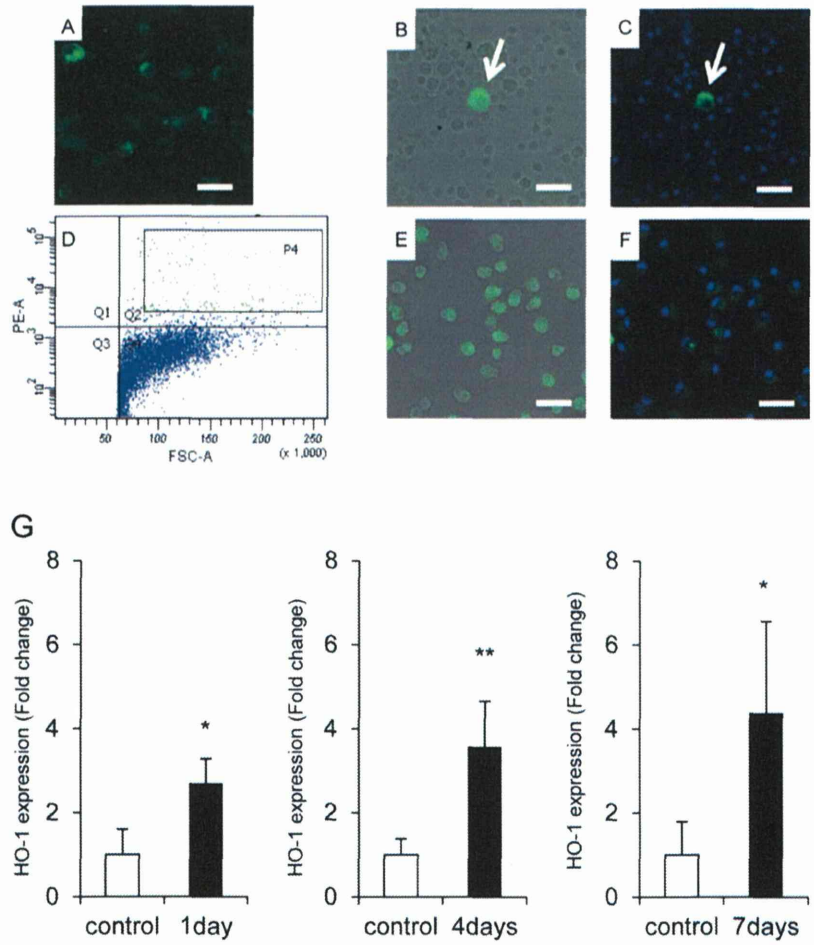

Fig. 1. RGC purification using FACS from dissociated retinas retrogradely labeled with 4Di-10ASP. **A:** Representative photograph of a flat-mount retina. The RGCs were labeled with 4Di-10ASP (green). **B,C:** Representative photographs of dissociated retinal cells before sorting. 0.2% of the cells were 4Di-10ASP+ RGCs before sorting. The arrows indicate RGCs. **D:** FACS analysis of retinal cells. **E,F:** Representative photographs of dissociated retinal cells after sorting. **G:** Graphs comparing RGC gene expression changes in control and NC mice. Changes were determined by qPCR measurements of mRNA levels in the RGCs. mRNA expression of *Ho-1* in the RGCs had increased 1 (control, n = 4; NC, n = 4), 4 (control, n = 5; NC, n = 5), and 7 (control, n = 4; NC, n = 5) days after NC. NC, nerve crush. $\star P < 0.05$, $\star\star P < 0.01$ Scale bars = 20 μm.

multiple groups were analyzed by using the Krüskal-Wallis, followed by Steel's, tests. Differences were considered statistically significant at $P < 0.05$.

RESULTS

Isolation of RGCs With FACS and Changes in RGC Gene Expression 7 Days After NC

RGCs were retrogradely labeled with 4Di-10ASP 7 days after NC (Fig. 1A). The ratio of 4Di-10ASP$^+$ RGCs in a sample of dissociated retinal cells before sorting was only 0.2% (Fig. 1B,C). Our FACS analysis showed that, before sorting, there were relatively few large and highly fluorescent cells in the dissociated retinas (Fig. 1D). Sorting greatly increased the proportion of these cells (Fig. 1E,F). We then examined post-NC changes in gene expression in these FACS-sorted RGCs. Table 1 shows the genes with the greatest increases in expression, as determined by microarray analysis. The expression of each of these genes increased twofold or more. We also examined the expression of the *Ho-1* gene in the purified RGCs with qPCR. Normalized to *Ho-1* expression levels in control RGCs, there were increases of 2.7 ± 0.58, 3.6 ± 1.1, and 4.4 ± 2.2 times, at 1, 4, and 7 days after NC, respectively. qPCR thus showed increased *Ho-1* expression in the RGCs at every stage following NC ($P < 0.05$, $P < 0.01$; Fig. 1G).

Immunohistochemical Detection of HO-1 After NC

HO-1 immunoreactivity was not observed in normal retinas (Fig. 2A). However, 1, 4, and 7 days after

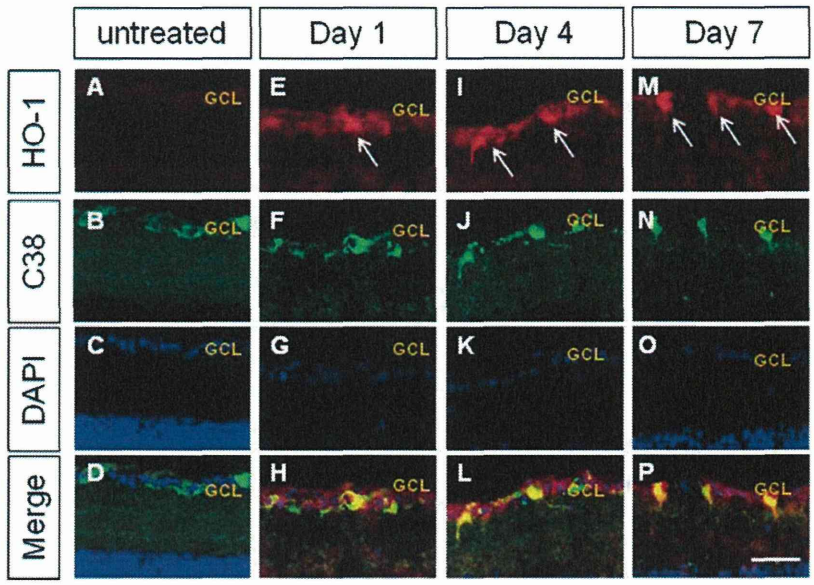

Fig. 2. Changes in HO-1 expression after NC. **A–D:** Normal retina. **E–H:** One day after NC. **I–L:** Four days after NC. **M–P:** Seven days after NC. HO-1 immunoreactivity was detected in the GCL 4 days and 7 days after NC. Arrows indicate HO-1 in the GCL. Scale bar = 50μm.

NC, immunostaining showed that HO-1-positive cells were present in the GCL (Fig. 2E,I,M). Double staining for HO-1 and C38 protein showed that the cells expressing HO-1 were all RGCs, although not all RGCs expressed HO-1 (Fig. 2H,L,P). We also found that, over time, the ratio of C38 protein-stained RGCs to DAPI-stained RGCs slowly decreased ($P < 0.05$; Fig. 3A). The proportion of HO-1 positive cells, however, rose significantly in the GCL after NC ($P < 0.05$; Fig. 3B). This tendency did not change near the optic nerve (500 μm) and far from it (1,000 μm).

CoPP Upregulated the Expression of HO-1 Protein

It is difficult to collect cells including protein because of their scarcity in the retina, especially after NC. We could not obtain enough protein in purified RGCs for immunoblot analysis, so we tried qPCR and immunoblot analysis in the retina. The levels of *Ho-1* mRNA in the retina did not increase after 1 or 2 days of CoPP administration (data not shown). However, 3 days of CoPP administration resulted in increased *Ho-1* mRNA expression. We therefore chose a CoPP treatment without NC lasting for 6 days. The levels of HO-1 protein in the retina also increased significantly 3 days after the injection of CoPP ($P < 0.05$; Fig. 4B). Additionally, immunofluorescence analysis showed that IP injection of CoPP induced expression of HO-1 in the GCL (Fig. 4C).

Effects of CoPP on Protection of RGCs From NC

Before NC, there was no significant difference in the density of FG-labeled RGCs in mice treated with vehicle (3,160 ± 435 cells/mm^2), CoPP (3,549 ± 475 cells/mm^2), or a combination of CoPP and SnPP (3,156 ± 658 cells/mm^2). Seven days after NC, the density of FG-labeled RGCs in the mice treated with CoPP was significantly higher than in those treated with vehicle (1,313 ± 137 cells/mm^2 and 868 ± 253 cells/mm^2, respectively, $P < 0.01$, $P < 0.05$), whereas the mice treated with a combination of CoPP and SnPP (808 ± 262 cells/mm^2) did not show a significant difference from those treated with vehicle (Fig. 5).

DISCUSSION

It is well known that axonal damage induces significant RGC death, but a small number of RGCs are nevertheless able to survive 7 days after NC. To search for new treatments for retinal diseases, we tried to identify patterns of change in the gene expression of these axonal-damage-resistant RGCs. A microarray assessment of sorted post-NC RGCs revealed that the expression of HO-1, in particular, increased significantly. Immunofluorescence analysis also revealed that a significantly higher proportion of HO-1-positive cells was present in the RGCs 1, 4, and 7 days after NC and that the ratio of HO-1-positive cells in the RGCs gradually increased during that time. Finally, an examination of retinas pretreated with CoPP, which is a nonsubstrate HO-1 inducer, revealed a higher density of surviving RGCs after NC, whereas retinas pretreated with both CoPP and SnPP showed no difference in RGC survival from the untreated group. These data strongly suggest that molecules expressed in surviving RGCs, especially HO-1, contribute to the survival of RGCs through a neuroprotective effect.

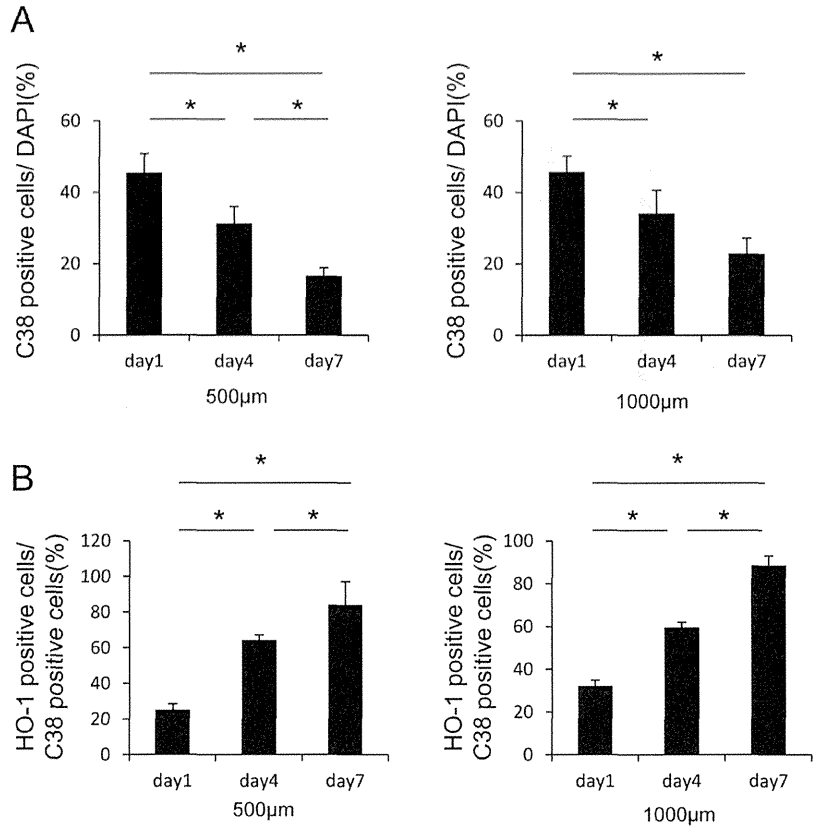

Fig. 3. Quantitative analysis of HO-1 positive cell numbers in the GCL after NC. The left and right graphs represent measurements in areas 500 μm and 1,000 μm from the center of the optic nerve, respectively. **A:** The ratio of C38 protein-stained RGCs to DAPI-stained RGCs (n = 4 in each group). **B:** The proportion of HO-1 positive cells to C38 protein-stained RGCs (n = 4 in each group). $*P < 0.05$.

RGCs represent only a small fraction of the total retinal cell population, so it is easy to overlook responses specific to them. To overcome this obstacle, we used FACS, a technique capable of identifying RGC-specific changes that has recently been introduced (Fischer et al., 2004). FACS functions by isolating RGCs from other cells and examining gene expression in them exclusively. Our experience indicates that a combination of sorting by retrograde fluorescent labeling and cell size is most useful in isolating the RGCs and allows us to obtain the purest samples. Moreover, in our previous research, cell sorting very clearly revealed markers specifically expressed by RGCs (Himori et al., 2013). The ratio of $4Di\text{-}10ASP^{+}$ RGCs to 4′-6-diamino-2-phenylindole $(DAPI)^{+}$ cells rose from only 0.2% to 96.4% with sorting (as shown in Fig. 1). This high level of purity gave us exceptionally large sample sizes for both the microarray and the qPCR analyses and allowed us to perform very effective statistical analyses of biological variations and obtain highly reliable results. The possibility remains, however, that our analysis was affected by the exclusion of small RGCs. Therefore, further experiments may be required to provide more precise results.

Our previous work showed that expression of *Ho-1* had increased 1 day after NC (Himori et al., 2013). Four days after NC, *Ho-1* continued to have a high level of expression. Seven days after NC, moreover, expression of *Ho-1* had increased still further. This study included a microarray analysis of the purified RGCs, which clearly showed high HO-1 expression in the surviving RGCs 7 days after NC. Approximately 7 days after NC, even though almost all the RGCs were disrupted by the apoptotic reaction, a fraction of cells survived. Although factors other than HO-1 might rise after injection of CoPP, we focused on HO-1 because many researchers have suggested that HO-1 has a strong cellular protective effect in RGCs and in Müller cells (Arai-Gaun et al., 2004; Sun et al., 2010). Increased levels of HO-1 protein have been observed in RGCs exposed to hydrostatic pressure in vitro and in mouse retinas exposed to acute elevated IOP (Liu et al., 2007). Hypothesizing that the neuroprotective factor after NC

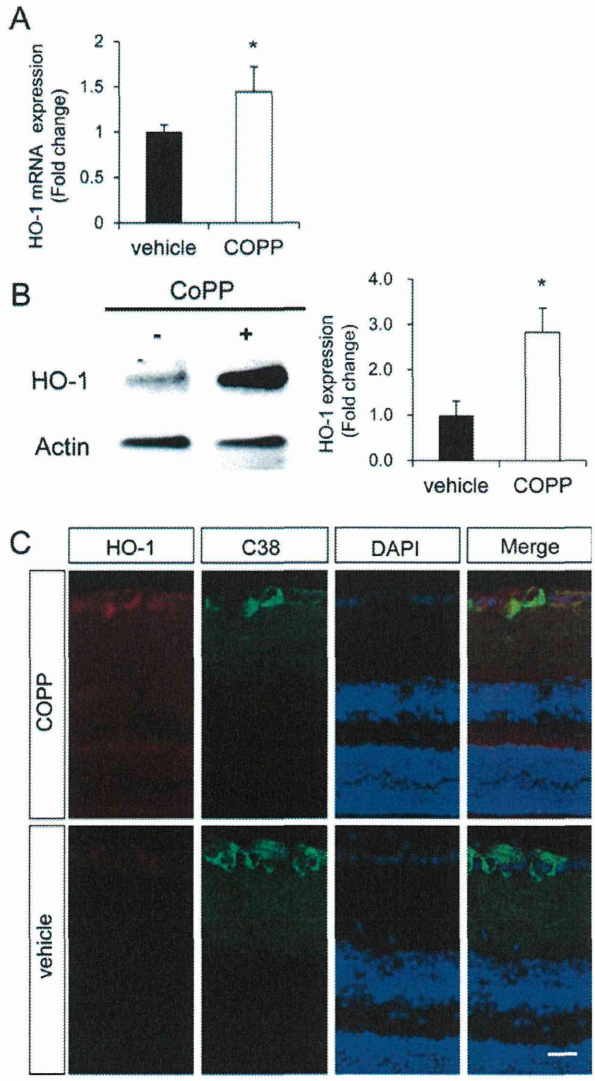

Fig. 4. **A**: The left graph shows qPCR data on *Ho-1* mRNA expression changes. **B:** Representative immunoblotting data, with antibodies for HO-1 and β-actin (top and bottom), on retinal HO-1 induction in mice pretreated with either vehicle or CoPP. The right graph shows the band intensities of HO-1 relative to β-actin, measured with densitometry (n = 3–4 in each group). $*P < 0.05$. **C:** Immunofluorescence images showing the localization pattern of HO-1 protein. HO-1 was detected only in the CoPP-pretreated retina without NC. Scale bar = 20μm.

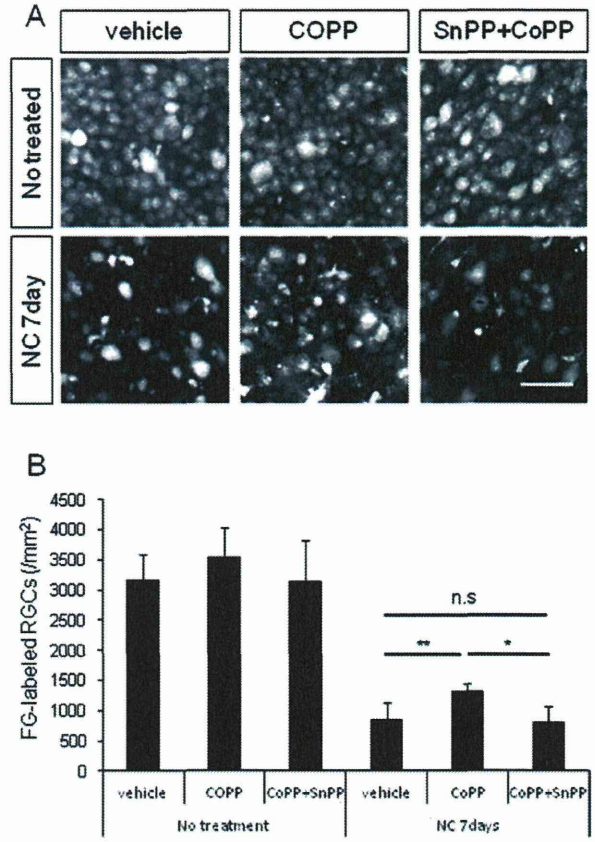

Fig. 5. Effect of HO-1 on RGC protection after NC. **A:** Representative photographs of RGCs in flat-mounted retinas. **B:** Quantitative data on the density of RGCs after NC (n = 4–7 in each group). $*P < 0.05$, $**P < 0.01$. Scale bar = 50μm.

was stronger in these surviving RGCs than in the apoptotic cells, we performed the microarray analysis, which revealed the high expression of HO-1. Additionally, experimental studies showed that free-radical scavengers effectively prevented glaucomatous tissue injury, including glutamate- and IOP-induced RGC death (Inomata et al., 2006; Munemasa et al., 2009). Oxidative stress is one of the most common stress signals inducing HO-1 expression, and it has been suggested that it plays a role in signaling RGC death in glaucoma (Tezel, 2006; Guo et al., 2011).

HO-1 belongs to the heat shock family of proteins, a group that can function as antioxidants, antiapoptotics, cytoprotectors, or anti-inflammatory agents in different pathologic conditions. The induction of HO-1 is regulated at the level of transcription by HSF1, AP-1, NFκβ, and Nrf2. Nrf2, in particular, has an important role in the expression of HO-1 (Naidu et al., 2009; Koriyama et al., 2010). Nrf2 normally resides in the cytoplasm bound by its cytosolic inhibitor, Keap1, which targets it for proteosomal degradation (Itoh et al., 1997, 1999). Our previous work suggested that the large quantity of ROS induced by NC disrupts the association of Nrf2 and Keap1, which leads to nuclear translocation of Nrf2 and the transcriptional activation of cytoprotective genes (Himori et al., 2013). We believe that mitochondrial dysfunction can induce the generation of ROS and that HO-1 is a key part of the antioxidant enzymes that form in response. Additionally, members of the Bcl2 gene family, including Bcl2, BclxL, and Bax, play an important role in regulating RGC death in glaucoma (Nickells et al., 2008). Cell

apoptosis stands out as one of the key parts of this biological process. In this study, microarray and qPCR analyses revealed that HO-1 is upregulated in the RGCs after NC. Although this might reflect only the nature of NC injury, pharmacological induction of HO-1 with CoPP has also been shown, in a previous study, to contribute to the reduction of RGC death and to play a beneficial role in retinal protection after ischemia–reperfusion injury (Sun et al., 2010). Sun et al. found that HO-1 was related to a reduction in the recruitment of macrophage infiltration in the retina through the suppression of monocyte chemoattractant protein. A different study showed that a combination of astrocytes and microglia could prevent excessive inflammatory responses in the brain by regulating microglial expression of HO-1 and production of ROS (Min et al., 2006). Similarly, HO-1 probably has a role in the inflammatory pathways involving NF-κB and MAPK signaling, which are present in a commonly used model of high-IOP-induced retinal ischemia. Previous reports have shown that HO-1 overexpression can suppress inflammatory responses such as NF-κB protein expression, inflammatory cytokine upregulation, and macrophage infiltration after high-IOP-induced retinal ischemia. We have also reported, from our previous research, that the upregulation of antioxidants via the Keap1–Nrf2 pathway was a very important part of the mechanism of cytoprotection (Himori et al., 2013). Building on our microarray analysis, our future research will include an ingenuity pathway analysis to determine the most closely related oxidative pathway involving HO-1.

In summary, microarray and qPCR data analyses indicated that RGC gene responses were closely linked to optic nerve injury in our mouse NC model. Neuroprotective strategies have been proposed and are being investigated as new goals for glaucoma therapy. Effective neuroprotection, aimed at salvaging functional RGCs and their axons before they are irreversibly damaged, requires early intervention and targeting of upstream events. Identification of the early clinical molecular events in RGCs would add to our understanding of the nature of glaucomatous injury and provide potential targets for neuroprotective strategies. This study demonstrates that inducing the overexpression of HO-1 may have promise as a neuroprotective treatment for glaucoma, and in particular for NTG, which is the most prevalent type of glaucoma in Asian countries.

ACKNOWLEDGMENTS

We thank Mr. Tim Hilts for reviewing and editing the language of the manuscript and Ms. Junko Sato for technical assistance. The C38 antibody was kindly provided by Drs. Takatoshi Wakabayashi and Jun Kosaka. The authors have no competing financial interests.

REFERENCE

Arai-Gaun S, Katai N, Kikuchi T, Kurokawa T, Ohta K, Yoshimura N. 2004. Heme oxygenase-1 induced in muller cells plays a protective role in retinal ischemia-reperfusion injury in rats. Invest Ophthalmol Vis Sci 45:4226–4232.

Ferreira SM, Lerner SF, Brunzini R, Reides CG, Evelson PA, Llesuy SF. 2010. Time course changes of oxidative stress markers in a rat experimental glaucoma model. Invest Ophthalmol Vis Sci 51:4635–4640.

Fischer D, Petkova V, Thanos S, Benowitz LI. 2004. Switching mature retinal ganglion cells to a robust growth state in vivo: gene expression and synergy with RhoA inactivation. J Neurosci 24:8726–8740.

Guo Y, Johnson EC, Cepurna WO, Dyck JA, Doser T, Morrison JC. 2011. Early gene expression changes in the retinal ganglion cell layer of a rat glaucoma model. Invest Ophthalmol Vis Sci 52:1460–1473.

Harada T, Harada C, Nakamura K, Quah HM, Okumura A, Namekata K, Saeki T, Aihara M, Yoshida H, Mitani A, Tanaka K. 2007. The potential role of glutamate transporters in the pathogenesis of normal tension glaucoma. J Clin Invest 117:1763–1770.

Himori N, Yamamoto K, Maruyama K, Ryu M, Taguchi K, Yamamoto M, Nakazawa T. 2013. Critical role of Nrf2 in oxidative stress-induced retinal ganglion cell death. J Neurochem 127:669–680.

Inomata Y, Nakamura H, Tanito M, Teratani A, Kawaji T, Kondo N, Yodoi J, Tanihara H. 2006. Thioredoxin inhibits NMDA-induced neurotoxicity in the rat retina. J Neurochem 98:372–385.

Itoh K, Chiba T, Takahashi S, Ishii T, Igarashi K, Katoh Y, Oyake T, Hayashi N, Satoh K, Hatayama I, Yamamoto M, Nabeshima Y. 1997. An Nrf2/small Maf heterodimer mediates the induction of phase II detoxifying enzyme genes through antioxidant response elements. Biochem Biophys Res Commun 236:313–322.

Itoh K, Wakabayashi N, Katoh Y, Ishii T, Igarashi K, Engel JD, Yamamoto M. 1999. Keap1 represses nuclear activation of antioxidant responsive elements by Nrf2 through binding to the amino-terminal Neh2 domain. Genes Dev 13:76–86.

Iwase A, Suzuki Y, Araie M, Yamamoto T, Abe H, Shirato S, Kuwayama Y, Mishima HK, Shimizu H, Tomita G, Inoue Y, Kitazawa Y, Tajimi Study Group JpGS. 2004. The prevalence of primary open-angle glaucoma in Japanese: the Tajimi Study. Ophthalmology 111: 1641–1648.

Izzotti A, Bagnis A, Saccà SC. 2006. The role of oxidative stress in glaucoma. Mutat Res 612:105–114.

Keyse SM, Tyrrell RM. 1989. Heme oxygenase is the major 32-kDa stress protein induced in human skin fibroblasts by UVA radiation, hydrogen peroxide, and sodium arsenite. Proc Natl Acad Sci U S A 86: 99–103.

Koriyama Y, Chiba K, Yamazaki M, Suzuki H, Muramoto K, Kato S. 2010. Long-acting genipin derivative protects retinal ganglion cells from oxidative stress models in vitro and in vivo through the Nrf2/antioxidant response element signaling pathway. J Neurochem 115:79–91.

Lai IR, Chang KJ, Tsai HW, Chen CF. 2008. Pharmacological preconditioning with simvastatin protects liver from ischemia-reperfusion injury by heme oxygenase-1 induction. Transplantation 85:732–738.

Lebrun-Julien F, Di Polo A. 2008. Molecular and cell-based approaches for neuroprotection in glaucoma. Optomol Vis Sci 85:417–424.

Li Volti G, Sorrenti V, Murabito P, Galvano F, Veroux M, Gullo A, Acquaviva R, Stacchiotti A, Bonomini F, Vanella L, Di Giacomo C. 2007. Pharmacological induction of heme oxygenase-1 inhibits iNOS and oxidative stress in renal ischemia-reperfusion injury. Transplant Proc 39:2986–2991.

Liu Q, Ju WK, Crowston JG, Xie F, Perry G, Smith MA, Lindsey JD, Weinreb RN. 2007. Oxidative stress is an early event in hydrostatic pressure induced retinal ganglion cell damage. Invest Ophthalmol Vis Sci 48:4580–4589.

Mancuso C. 2004. Heme oxygenase and its products in the nervous system. Antiox Redox Signal 6:878–887.

Min KJ, Yang MS, Kim SU, Jou I, Joe EH. 2006. Astrocytes induce hemeoxygenase-1 expression in microglia: a feasible mechanism for preventing excessive brain inflammation. J Neurosci 26:1880–1887.

Munemasa Y, Ahn JH, Kwong JM, Caprioli J, Piri N. 2009. Redox proteins thioredoxin 1 and thioredoxin 2 support retinal ganglion cell survival in experimental glaucoma. Gene Ther 16:17–25.

Naidu S, Vijayan V, Santoso S, Kietzmann T, Immenschuh S. 2009. Inhibition and genetic deficiency of p38 MAPK up-regulates heme oxygenase-1 gene expression via Nrf2. J Immunol 182:7048–7057.

Nakazawa T, Nakazawa C, Matsubara A, Noda K, Hisatomi T, She H, Michaud N, Hafezi-Moghadam A, Miller JW, Benowitz LI. 2006. Tumor necrosis factor-alpha mediates oligodendrocyte death and delayed retinal ganglion cell loss in a mouse model of glaucoma. J Neurosci 26:12633–12641.

Nakazawa T, Hisatomi T, Nakazawa C, Noda K, Maruyama K, She H, Matsubara A, Miyahara S, Nakao S, Yin Y, Benowitz L, Hafezi-Moghadam A, Miller JW. 2007. Monocyte chemoattractant protein 1 mediates retinal detachment-induced photoreceptor apoptosis. Proc Natl Acad Sci U S A 104:2425–2430.

Nakazawa T, Shimura M, Ryu M, Nishida K, Pagès G, Pouysségur J, Endo S. 2008. ERK1 plays a critical protective role against N-methyl-D-aspartate-induced retinal injury. J Neurosci Res 86:136–144.

Neufeld AH, Sawada A, Becker B. 1999. Inhibition of nitric-oxide synthase 2 by aminoguanidine provides neuroprotection of retinal ganglion cells in a rat model of chronic glaucoma. Proc Natl Acad Sci U S A 96:9944–9948.

Nickells RW, Semaan SJ, Schlamp CL. 2008. Involvement of the Bcl2 gene family in the signaling and control of retinal ganglion cell death. Prog Brain Res 173:423–435.

Panagis L, Zhao X, Ge Y, Ren L, Mittag TW, Danias J. 2010. Gene expression changes in areas of focal loss of retinal ganglion cells in the retina of DBA/2J mice. Invest Ophthalmol Vis Sci 51:2024–2034.

Peng PH, Ko ML, Chen CF, Juan SH. 2008. Haem oxygenase-1 gene transfer protects retinal ganglion cells from ischaemia/reperfusion injury. Clin Sci 115:335–342.

Peng PH, Chao HM, Juan SH, Chen CF, Liu JH, Ko ML. 2011. Pharmacological preconditioning by low dose cobalt protoporphyrin induces heme oxygenase-1 overexpression and alleviates retinal ischemia-reperfusion injury in rats. Curr Eye Res 36:238–246.

Quigley HA. 1996. Number of people with glaucoma worldwide. Br J Ophthalmol 80:389–393.

Ryu M, Yasuda M, Shi D, Shanab AY, Watanabe R, Himori N, Omodaka K, Yokoyama Y, Takano J, Saido T, Nakazawa T. 2012. Critical role of calpain in axonal damage-induced retinal ganglion cell death. J Neuroscience Res 90:802–815.

Shanab AY, Nakazawa T, Ryu M, Tanaka Y, Himori N, Taguchi K, Yasuda M, Watanabe R, Takano J, Saido T, Minegishi N, Miyata T, Abe T, Yamamoto M. 2012. Metabolic stress response implicated in diabetic retinopathy: the role of calpain, and the therapeutic impact of calpain inhibitor. Neurobiol Dis 48:556–567.

Shibahara S, Müller RM, Taguchi H. 1987. Transcriptional control of rat heme oxygenase by heat shock. J Biol Chem 262:12889–12892.

Steele MR, Inman DM, Calkins DJ, Horner PJ, Vetter ML. 2006. Microarray analysis of retinal gene expression in the DBA/2J model of glaucoma. Invest Ophthalmol Vis Sci 47:977–985.

Sullivan RK, Woldemussie E, Macnab L, Ruiz G, Pow DV. 2006. Evoked expression of the glutamate transporter GLT-1c in retinal ganglion cells in human glaucoma and in a rat model. Invest Ophthalmol Vis Sci 47:3853–3859.

Sun MH, Pang JH, Chen SL, Han WH, Ho TC, Chen KJ, Kao LY, Lin KK, Tsao YP. 2010. Retinal protection from acute glaucoma-induced ischemia-reperfusion injury through pharmacologic induction of heme oxygenase-1. Invest Ophthalmol Vis Sci 51:4798–4808.

Takeda A, Onodera H, Sugimoto A, Itoyama Y, Kogure K, Shibahara S. 1994. Increased expression of heme oxygenase mRNA in rat brain following transient forebrain ischemia. Brain Res 666:120–124.

Tezel G. 2006. Oxidative stress in glaucomatous neurodegeneration: mechanisms and consequences. Prog Ret Eye Res 25:490–513.

Uchibayashi R, Tsuruma K, Inokuchi Y, Shimazawa M, Hara H. 2011. Involvement of Bid and caspase-2 in endoplasmic reticulum stress- and oxidative stress-induced retinal ganglion cell death. J Neurosci Res 89: 1783–1794.

Wakabayashi T, Kosaka J, Mochii M, Miki Y, Mori T, Takamori Y, Yamada H. 2010. C38, equivalent to BM88, is developmentally expressed in maturing retinal neurons and enhances neuronal maturation. J Neurochem 112:1235–1248.

Weber AJ, Harman CD, Viswanathan S. 2008. Effects of optic nerve injury, glaucoma, and neuroprotection on the survival, structure, and function of ganglion cells in the mammalian retina. J Physiol 586:4393–4400.

Yuki K, Ozawa Y, Yoshida T, Kurihara T, Hirasawa M, Ozeki N, Shiba D, Noda K, Ishida S, Tsubota K. 2011. Retinal ganglion cell loss in superoxide dismutase 1 deficiency. Invest Ophthalmol Vis Sci 52:4143–4150.

Yücel YH, Zhang Q, Weinreb RN, Kaufman PL, Gupta N. 2003. Effects of retinal ganglion cell loss on magno-, parvo-, koniocellular pathways in the lateral geniculate nucleus and visual cortex in glaucoma. Prog Ret Eye Res 22:465–481.